Rac1/RhoA antagonism defines cell-to-cell heterogeneity during epidermal morphogenesis in nematodes

Emmanuel Martin, Marie-Hélène Ouellette, and Sarah Jenna

Department of Chemistry, Pharmaqam, Université du Québec à Montréal, Montreal, QC H3C 3P8, Canada

The antagonism between the GTPases Rac1 and RhoA controls cell-to-cell heterogeneity in isogenic populations of cells in vitro and epithelial morphogenesis in vivo. Its involvement in the regulation of cell-to-cell heterogeneity during epidermal morphogenesis has, however, never been addressed. We used a quantitative cell imaging approach to characterize epidermal morphogenesis at a single-cell level during early elongation of *Caenorhabditis elegans* embryos. This study reveals that a Rac1-like pathway, involving the Rac/Cdc42 guanine-exchange factor β-PIX/PIX-1 and effector PAK1/PAK-1, and a RhoA-like pathway, involving ROCK/LET-502, control the remodeling of apical junctions and the formation of basolateral protrusions in distinct subsets of hypodermal cells. In these contexts, protrusions adopt lamellipodia or an amoeboid morphology. We propose that lamella formation may reduce tension building at cell–cell junctions during morphogenesis. Cell-autonomous antagonism between these pathways enables cells to switch between Rac1- and RhoA-like morphogenetic programs. This study identifies the first case of cell-to-cell heterogeneity controlled by Rac1/RhoA antagonism during epidermal morphogenesis.

Introduction

Morphogenesis of epithelial cells is involved in organogenesis during embryonic development, organ regeneration, and metastasis of carcinoma cells. The remodeling of apical junctions leading to apical constriction or anisotropic rearrangement of apical junctions was shown to drive epithelial morphogenesis during gastrulation, planar cell intercalation, and elongation in a number of genetic models from the nematode to the mouse (Munjal and Lecuit, 2014). Junction shrinkage has been mostly investigated during epithelial cell intercalation leading to the elongation of *Drosophila melanogaster* germ band (Lecuit and Yap, 2015). Myosin II and its upstream regulator, the RhoA effector ROCK, play a central role in these processes through the regulation of cadherin endocytosis from the adherens junctions (Bertet et al., 2004; Levayer et al., 2011; Yashiro et al., 2014; Collinet et al., 2015). Epithelial morphogenesis was also shown to involve the formation of basolateral protrusions in a polarized manner. These protrusions have been proposed to set the polarity of elongation/intercalation in nematodes, arthropods, and mice (Heid et al., 2001; Ewald et al., 2008; Georgiou and Baum, 2010; Williams et al., 2014; Walck-Shannon et al., 2015). Studies using epithelial cell culture and developmental systems revealed that myosin contraction at the apical junctions and at the protrusions, which constitute the principal motors for cell-shape changes during morphogenesis, depends on the activation of two main pathways controlled by the Rho GTPases Rac1 and RhoA (Vaezi et al., 2002; Yu et al., 2003; Vargo-Gogola et al., 2006). Interestingly, pathways involving these two GTPases tend to function in an antagonistic manner (Chauhan et al., 2011; Guilluy et al., 2011; Vlachos and Harden, 2011). For instance, this antagonism was shown to generate distinct and mutually exclusive Rac1 and RhoA subcellular compartments in placode cells, controlling invagination of the epithelium during lens development in mice (Chauhan et al., 2011). It was also shown to allow invasive carcinoma cells to switch between a Rac1-dependent mesenchymal to a RhoA-dependent amoeboid invasion mode in response to increased stiffness of cell environment (Yamazaki et al., 2009). Recent studies using automated single-cell analysis demonstrated that switching between Rac1 and RhoA programs enables cells of an isogenic population to move within a defined landscape composed of several discrete shapes (Yin et al., 2013; Sailem et al., 2014). Importantly, these studies suggested that this morphological heterogeneity may facilitate population-level behavior and survival when exposed to environmental changes (Yin et al., 2013; Sailem et al., 2014). Although cell-to-cell heterogeneity within an isogenic population of mesenchymal cells is now well accepted, the presence of such heterogeneity between cells of a polarized epithelium

Correspondence to Sarah Jenna: jenna.sarah@uqam.ca

Abbreviations used: AD, average deformation; RDR, relative deformation rate; TDA, transversal junction between dorsal anterior cells; TLA, transversal junction between lateral anterior cells; TLP, transversal junction between lateral posterior cells; TVA, transversal junction between ventral anterior cells; TVP, transversal junction between ventral posterior cells; wt, wild-type.

The Rockefeller University Press $30.00
J. Cell Biol. Vol. 215 No. 4 483–498
https://doi.org/10.1083/jcb.201604015

has not yet been observed. Intriguingly, columnar epithelial cells display an evolutionarily conserved distribution of polygonal shapes, with a peak of 40 to 45% hexagons (Lewis, 1928; Gibson et al., 2006; Gibson and Gibson, 2009). A recent study using human keratinocytes revealed that this rate of hexagons depends on deterministic instead of stochastic mechanisms and, more particularly, on cell–cell junction remodeling by the RhoA effectors ROCK1 and ROCK2 (Kalaji et al., 2012). Overall, these studies suggest that distribution of shapes within an epithelium may depend on signaling pathways previously shown to control epithelial morphogenesis. Consequently, they raise an important and still unaddressed question: does Rac1/RhoA antagonism, which controls both epithelial morphogenesis and cell-to-cell heterogeneity within populations of mesenchymal cells, also define cell-to-cell heterogeneity during epithelial morphogenesis?

Embryonic elongation, a developmental stage of epidermal morphogenesis in *Caenorhabditis elegans*, is divided into an early and a late phase. Early elongation consists in a reduction of the diameter of the embryo and its elongation along its anteroposterior axis. At that stage, the hypodermis is composed of dorsal, lateral, and ventral hypodermal cells (Costa et al., 1998). Early elongation was proposed to result from the apical constriction of lateral hypodermal cells (Priess and Hirsh, 1986; Keller, 2006; Diogon et al., 2007). Rac1- and RhoA-like pathways involving the Rac/Cdc42 regulator and effector PIX-1/β-PIX and PAK-1/PAK1 and the RHO-1/RhoA effector LET-502/ROCK, respectively, were shown to control early elongation in parallel (Piekny et al., 2003; Gally et al., 2009; Martin et al., 2014). The RHO-1/LET-502 pathway is expected to be active in lateral cells and inactive in dorsal and ventral cells because of the expression of a RHO-1–specific GTPase-activating protein, RGA-2, in the latter cells (Diogon et al., 2007). The cells expressing active PIX-1 and PAK-1 are still unknown. This pathway was, however, suggested to mostly control morphogenetic processes at the anterior part of the embryo (Martin et al., 2014). Altogether, these studies suggest that the hypodermal cells may use different combinations of Rac1/RhoA signaling pathways along the dorsoventral and anteroposterior axes of the embryo during early elongation.

We used a quantitative imaging approach to characterize early elongation at a single-cell level. This study reveals that the PIX-1/PAK-1 pathway controls the remodeling of apical junctions and the formation of basolateral protrusions in dorsal anterior cells, whereas LET-502 controls similar processes in lateral cells. We also show that cells can switch between Rac1-like and RhoA-like morphogenetic programs upon genetic alteration of *let-502*, *pix-1*, or *pak-1*. We propose a model in which cell-autonomous Rac1/RhoA antagonism defines the morphogenetic program adopted by polarized epithelial cells and controls cell-to-cell heterogeneity during epithelial morphogenesis.

Results

Hypodermal cells follow different morphogenetic programs during early elongation

We used a quantitative imaging method to better assess the spatial distribution of cellular and molecular processes controlled by PIX-1/PAK-1 and LET-502 during early elongation. This method uses high-resolution four-dimensional confocal microscopy to measure the extent and nature of the deformation (elongation or shrinking) of cell–cell junctions between hypodermal cells during early elongation. These measurements were done in transgenic animals expressing the junction marker AJM-1::GFP and the F-actin–binding probe VAB-10(ABD)::mCherry in the hypodermis. AJM-1 is a protein partner of DLG-1/MAGUK/Discs large, being part of the apical junctional DLG-1/AJM-1 complex (Pásti and Labouesse, 2014). These transgenic animals displayed elongation rates and morphology similar to those of wild-type (wt) embryos during early elongation (Fig. S1).

AJM-1::GFP allowed us to measure the length of the transversal junctions between lateral anterior cells (TLA; Fig. 1, A and B, light red) and lateral posterior cells (TLP; Fig. 1 B, dark red); between dorsal anterior cells (TDA; Fig. 1, A and B, green) before and after fusion of dorsal 1 and 2 cells; and between ventral anterior cells (TVA; Fig. 1, A and B, light blue) and ventral posterior cells (TVP; Fig. 1 B, dark blue) at two different time points during early elongation (see Materials and methods; Figs. 1 A and S2). We also measured the length of longitudinal junctions between dorsal anterior cells and lateral anterior (Fig. 1 C, LDA, yellow) and posterior cells (LDP, orange) and between lateral and ventral anterior cells (LVA, light purple) and ventral posterior cells (LVP, dark purple). The average deformation (AD; in micrometers per minute) was computed for groups of junctions (Fig. 1, B and C). Positive AD values indicate that junctions elongate, whereas negative values indicate that junctions shrink during early elongation. Note that although TLA junction L2 (Fig. 1 A) displayed a constant deformation rate throughout early elongation (Fig. S3), we cannot exclude the possibility that this might not be the case for all cell–cell junctions in different genetic backgrounds. The deformation measured here may consequently slightly differ from the deformation rate of junctions at given times during morphogenesis.

This analysis revealed that TLA (Fig. 1 B, light red) shrank 2.5-fold faster than TLP (Fig. 1 B, dark red). In contrast, TVA (Fig. 1 B, light blue) shrank 3.5-fold less than TVP (dark blue). A small elongation was also measured for TDA (Fig. 1 B, green). Because dorsal posterior cells fuse during early elongation, AD could not be measured for the transversal junction between dorsal posterior cells (TDP; Fig. 1 B). These results suggest that the reduction of the head width of the embryo is mostly associated with the shrinking of transversal junctions of lateral hypodermal cells. However, these data also suggest that morphogenesis of the posterior part of the embryos depends on the shrinking of the transversal junctions of both lateral and ventral cells. These data deviate from the accepted model, suggesting that ventral cells may passively contribute to early elongation (Diogon et al., 2007).

When considering the deformation of cell–cell junctions between anterior cells individually (Fig. 1 D), we identified two set of junctions that are semi-aligned or aligned along the dorsoventral axis of the embryo (Fig. 1, A and D): the D1/L1/V1 junctions linking dorsal 1/2, lateral H1, and ventral 18/19 to their anterior neighbors and the junctions D2/L2/V2 linking those cells with their posterior neighbors (Fig. 1 A). Interestingly, these junctions appear to deform differently. For example, the D2 junctions elongate significantly less than D1 (*t* test, P = 0.004; Fig. 1 D). These data suggest that cell–cell junctions between dorsal 1/2 and their anterior and posterior neighbors use different morphogenetic mechanisms.

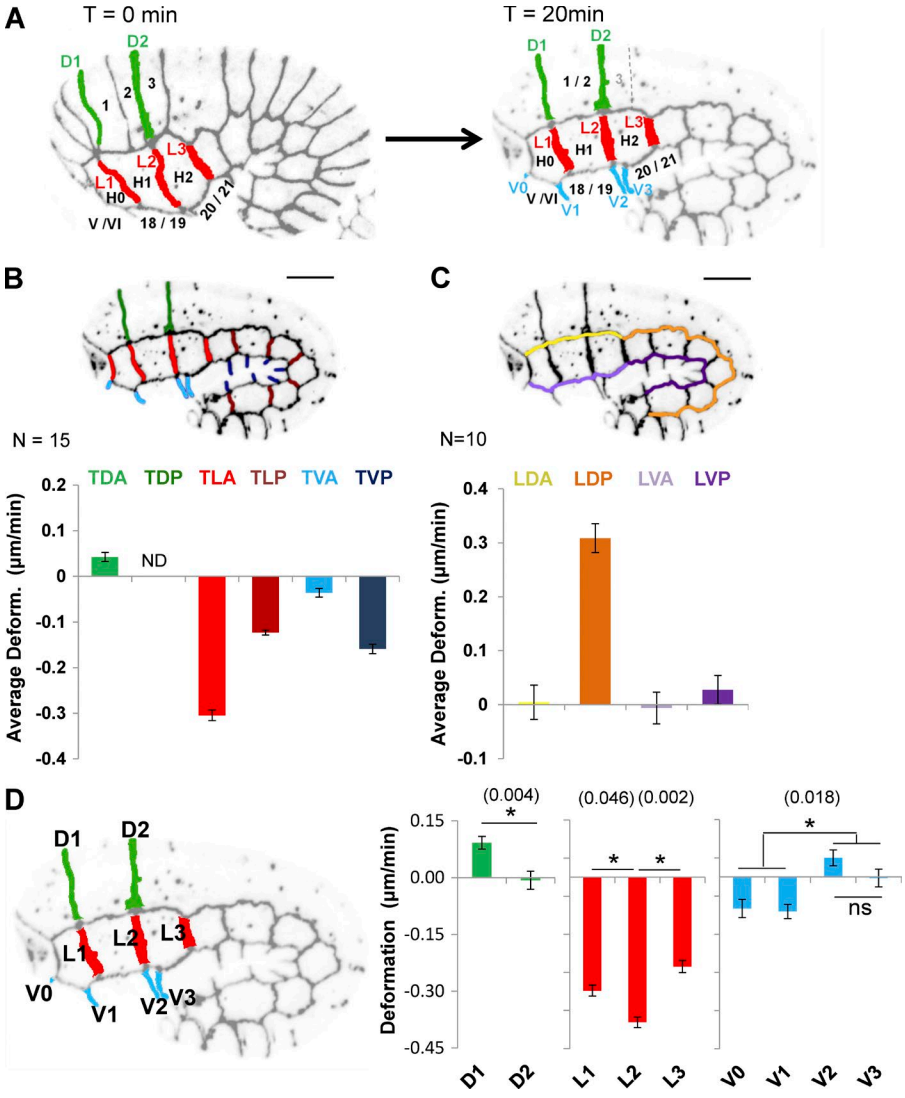

Figure 1. **Hypodermal cells follow different morphogenetic programs during early elongation.** (A) Identification of anterior dorsal (green), lateral (red), and ventral (blue) hypodermal cells and their cell–cell junctions. Bar graph representing the AD (in micrometers per minute) of groups of transversal (B) and longitudinal (C) junctions identified in embryos expressing AJM-1::GFP and VAB-10(ABD)::mCherry. The junctions are indicated by color coding: transversal junction between dorsal posterior cells (TDP), dark green; TDA, light green; TLA, light red; TLP, dark red; TVA, light blue; and TVP, dark blue; longitudinal junctions between dorsal anterior cells (LDA), yellow; dorsal posterior cells (LDP), orange; ventral anterior cells (LVA), light purple; and ventral posterior cells (LVP), dark purple. Positive AD values indicate that junctions elongate; negative values, that they shrink. $N \geq 10$ embryos were analyzed for each junction. (D) Bar graphs representing deformation of individual transversal anterior junctions in micrometers per minute. ND, not determined; ns, not significant; p-values (*) for significant *t* test are indicated in parentheses. Error bars indicate SEM.

LET-502 and PIX-1/PAK-1 control morphogenesis in different subsets of hypodermal cells

The results support the hypothesis that hypodermal cells follow different morphogenetic programs during early elongation. To better understand the genetic basis of this heterogeneity, we measured the AD of groups of hypodermal cell–cell junctions in embryos carrying the strong loss-of-function *let-502(sb118ts)* thermosensitive allele and grown at the restrictive temperature of 25.5°C, in *let-502(RNAi)* and wt animals (Fig. 2, A and B, left and middle). We also computed the relative deformation rate (RDR) for individual junctions of mutant/RNAi-treated animals compared with wt (see Materials and methods; Fig. 2, A and B, right). When considered at the organism level, *let-502(RNAi)* and *let-502(sb118ts)* embryos grown at 25.5°C displayed similar elongation defects (Fig. S4). They also displayed similar ADs and RDRs compared with wt (Fig. 2, A and B), consisting in a significant reduction of the shrinking of TLA, TLP, and TVP compared with wt animals (*t* test, $P < 0.045$; Fig. 2, A and B). This analysis also revealed that the RDRs (relative to wt) of these junctions were similar (~1.3) in *let-502(sb118ts)* and *let-502(RNAi)* embryos (Fig. 2, A and B, right). This suggests that *let-502* controls the shrinking of transversal membranes of lateral and ventral posterior cells in a manner similar to that previously suggested (Martin et al., 2014).

We also measured AD and RDR for cell–cell junctions in embryos carrying *pix-1(gk416)* and *pak-1(ok448)* null alleles (Fig. 2, C and D). These embryos displayed a significantly increased RDR over wt only at the anterior part of the embryos, consisting in the elongation of TDA and TVA junctions (*t* test, $P < 0.01$; Fig. 2, C and D). These results support previous studies suggesting that the *pix-1/pak-1* pathway controls early elongation mostly at the anterior part of the embryo (Martin et al., 2014). Note that D2/V2 junctions display higher RDRs than D1/V1 (Fig. 2, C and D, right), suggesting that morphogenetic differences observed for the anterior and posterior junctions of H1 lateral cells (Fig. 1 D) are also observed at dorsal and ventral cells and involve the function of *pix-1* and *pak-1*.

Altogether, these data suggest that *let-502* controls the deformation of transversal junctions of anterior and posterior lateral cells and ventral posterior cells, whereas *pix-1* and *pak-1* control the deformation of transversal junctions of dorsal and ventral anterior cells. These data also suggest that whereas *let-502* controls junction shrinking similarly in lateral (anterior and posterior) and ventral posterior cells, *pix-1* and *pak-1* function in a more spatially restricted manner, with a prominent function observed at the D2/V2 transversal junctions.

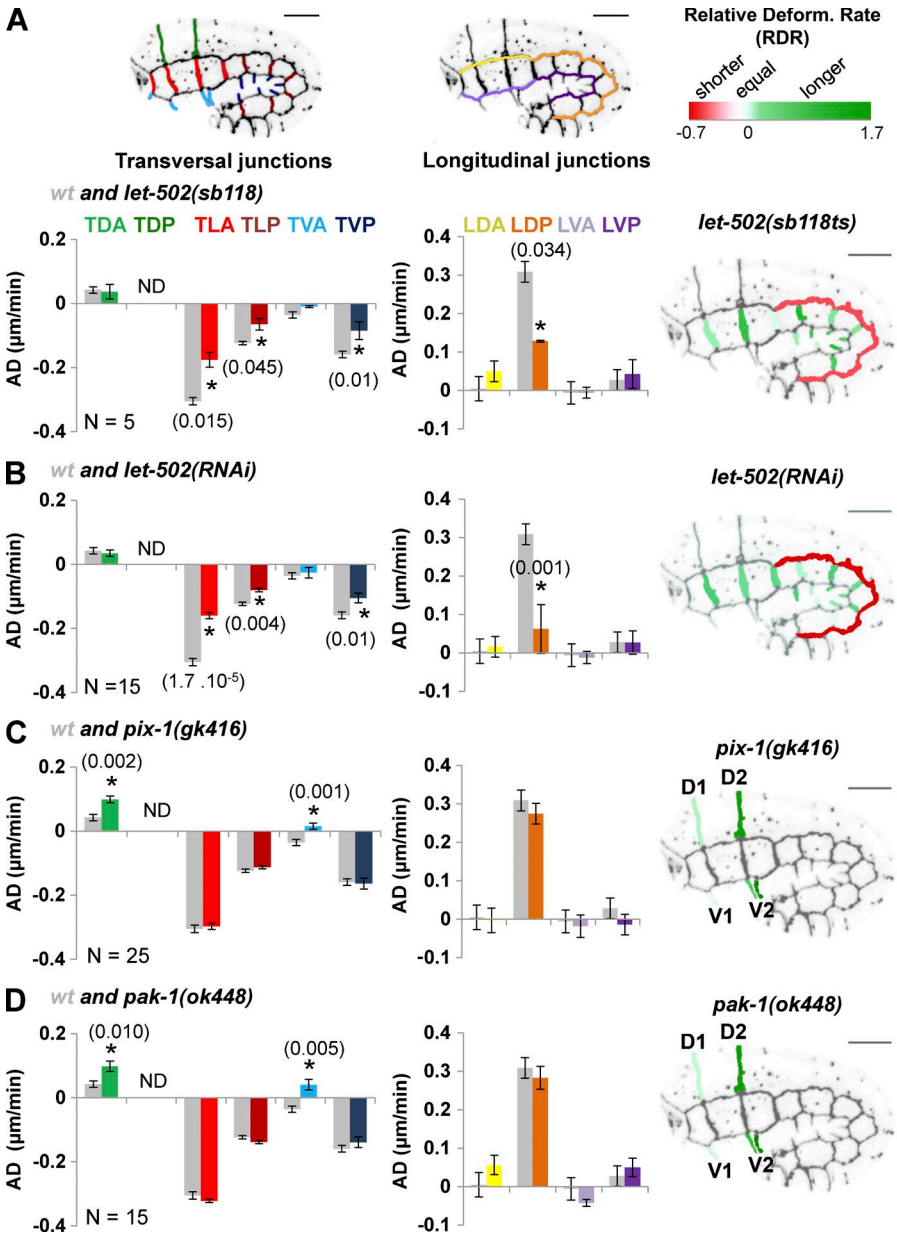

Figure 2. ***let-502*and *pix-1/pak-1* control the morphogenesis of different sets of hypodermal cells.** Bar graphs representing the AD (in micrometers per minute) of cell–cell junctions in *let-502(sb118ts)* (A), *let-502(RNAi)* (B), *pix-1(gk416)* (C), and *pak-1(ok448)* (D) embryos expressing AJM-1::GFP and VAB-10(ABD)::mCherry. Gray bar graphs in A–D represent AD measured for groups of junctions in wt embryos. The junctions are indicated in the embryo and bar graphs by color coding: transversal junction between dorsal posterior cells (TDP), dark green; TDA, light green; TLA, light red; TLP, dark red; TVA, light blue; and TVP, dark blue; longitudinal junctions between dorsal anterior cells (LDA), yellow; dorsal posterior cells (LDP), orange; ventral anterior cells (LVA), light purple; and ventral posterior cells (LVP), dark purple. Positive AD values indicate that junctions elongate; negative values, that they shrink. $N > 5$ embryos were analyzed per genotype and junction. Right, RDRs for mutants versus wt. ND, not determined; p-values from significant *t* test (*) are indicated in parentheses. Error bars indicate SEM.

let-502 and *pix-1/pak-1* pathways control the reorganization of apical junctions in distinct sets of hypodermal cells

Junction shrinking has been described in *D. melanogaster* to result from cortical contraction of myosin and assembly of higher-order complexes of junction proteins and their endocytosis (Bertet et al., 2004; Rauzi et al., 2008). Because myosin contraction was proposed to occur downstream of LET-502 mainly in lateral cells during early elongation in *C. elegans* (Diogon et al., 2007), we assessed whether PIX-1 and PAK-1 may control myosin contraction in dorsal and ventral cells and formation of higher-order complexes of junction proteins leading to cell–cell junction deformation. The anisotropy of fluorescently tagged junction proteins—the ratio of the maximal versus the minimal intensity of fluorescence measured along the junctions—was shown to correlate significantly with myosin-dependent tension applied to the junctions in mammalian systems (Engl et al., 2014). We thus measured the anisotropy of AJM-1::GFP at the transversal lateral junctions of wt embryos (Fig. 3, A and B). This revealed that AJM-1::GFP anisotropy significantly negatively correlated with the shrinking rate of these junctions (Spearman correlation coefficient = −0.98; $P = 3.9 \times 10^{-4}$; Fig. 3 B). To assess whether the level of AJM-1::GFP anisotropy depends on the tension applied to the junction, we measured this anisotropy at the lateral anterior transversal junctions (L1, L2, and L3) in wt embryos and embryos carrying a thermosensitive allele of the myosin heavy-chain coding gene *nmy-2(ne1490ts)*, at both permissive and restrictive temperature (18°C and 25°C, respectively; Fig. 3, A and C). This study revealed that AJM-1::GFP anisotropy was significantly reduced at the junctions upon inactivation of *nmy-2* (Fig. 3, A and C). Although the structure of the apical junction may be only indirectly modified by myosin contraction, these data identify AJM-1::GFP anisotropy as a powerful metric to measure myosin contraction-dependent remodeling of apical junctions during early elongation.

AJM-1::GFP anisotropy was measured for the transversal junctions between anterior hypodermal cells in wt, *let-502(RNAi)*, *pix-1(gk416)*, and *pak-1(ok448)* embryos (Fig. 4). This anisotropy was significantly reduced at D2 junctions between dorsal

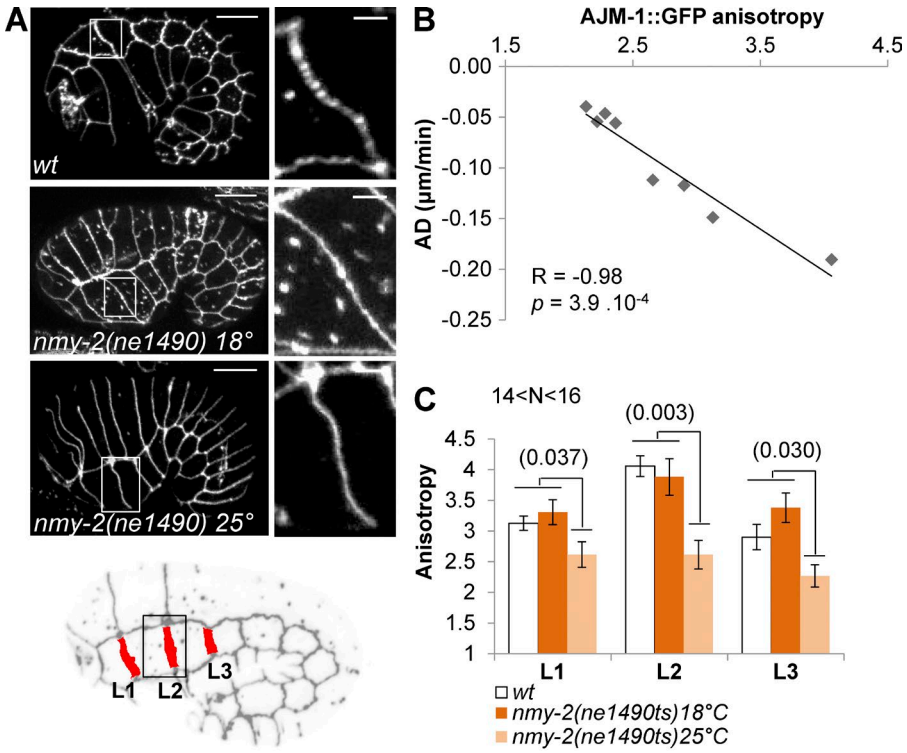

Figure 3. **AJM-1::GFP anisotropy is indicative of the level of myosin-dependent cell–cell junction remodeling.** (A) *z*-projections of confocal images of AJM-1::GFP expressed in wt and *nmy-2(ne1490ts)* at 18°C or 25°C. Locations of the enlarged image (right) are indicated by a white box. Bar: 10 µm; (enlarged image) 2 µm. L1–3 transversal lateral anterior junctions are identified in the embryo (B). Scatter plot expressing the AD of transversal junctions between lateral cells with respect to the mean AJM-1::GFP anisotropy measured for corresponding junctions. The Spearman correlation test (*R*) and corresponding p-value are indicated. (C) AJM-1::GFP anisotropy at lateral L1, L2, and L3 junctions of *ajm-1::GFP; vab-10(ABD)::mCh* (wt) and *nmy-2(ne1490ts); ajm-1::GFP* embryos at 18°C and 25°C. Significant *t* test p-values are indicated in parentheses. Error bars indicate SEM. *N* > 14 embryos were analyzed per genotype and junction.

cells in *pix-1(gk416)* and *pak-1(ok448)* but not *let-502(RNAi)* embryos (Fig. 4 A). In contrast, it was significantly reduced at L1 and L2 junctions between lateral cells in *let-502(RNAi)* but not *pix-1* and *pak-1* mutants (Fig. 4 B). No significant variation of AJM-1::GFP anisotropy was observed at ventral anterior junctions of tested animals (Fig. 4 C). These data suggest that *pix-1* and *pak-1* control the D2 junction remodeling between anterior dorsal cells, whereas *let-502* controls the L1 and L2 junction remodeling between lateral anterior cells.

Dorsal and lateral hypodermal cells produce convergent lamellipodia and amoeboid-like protrusions during early elongation

Epithelial morphogenesis was shown to involve the formation of basolateral protrusions during both dorsal intercalation and ventral enclosure in *C. elegans* (Williams-Masson et al., 1997, 1998). However, the potential involvement of such protrusions during early elongation has never been investigated. The mammalian orthologs of PIX-1 and PAK-1 were shown to control

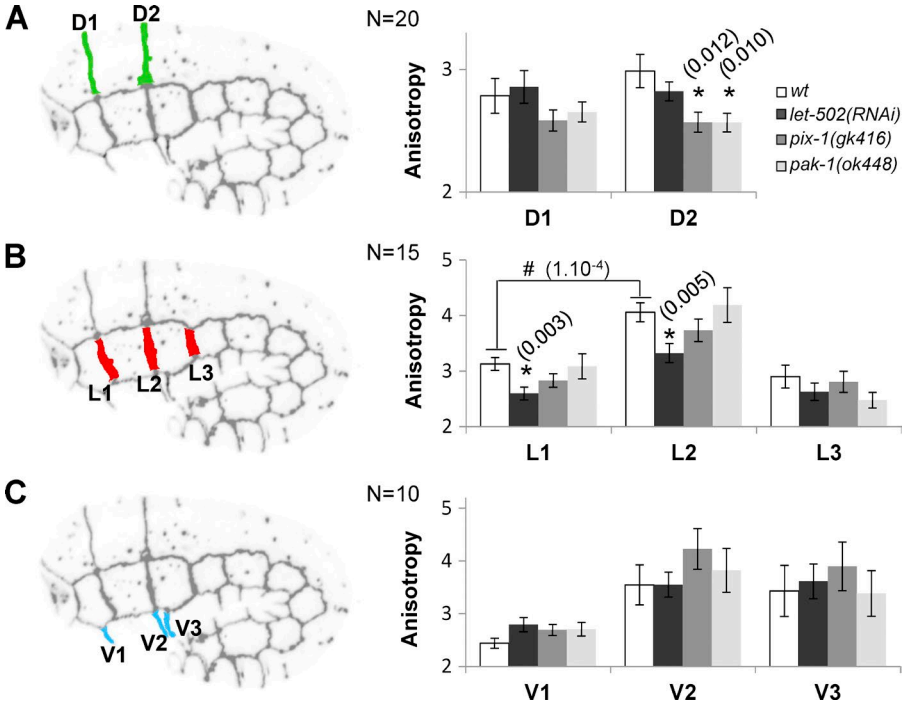

Figure 4. ***let-502*and *pix-1/pak-1* control the remodeling of the apical junctions between lateral and dorsal cells, respectively.** Mean of AJM-1::GFP anisotropy measured for junction between dorsal (A), lateral (B), and ventral (C) anterior cells in wt, *let-502(RNAi)*, *pix-1(gk416)*, and *pak-1(ok448)* embryos expressing AJM-1::GFP and VAB-10(ABD)::mCherry. *N* > 10 embryos were analyzed per genotype and junction. Significant *t* test p-values are indicated in parentheses. *, *t* test p-value significantly different from wt; #, *t* test p-value significantly different between L1 and L2 junctions in wt. Error bars indicate SEM.

formation of actin-rich protrusions during cell migration (Nayal et al., 2006). To better characterize the function of these genes during early elongation, we assessed whether they may be involved in the formation of basolateral protrusions by hypodermal cells. To do so, photobleaching of the F-actin–binding probes VAB-10(ABD)::mCherry in a selected subset of cells was used to observe the formation of protrusions by different groups of hypodermal cells. This revealed that dorsal 1/2 cells (Fig. 1 A) produce polarized and highly dynamic lamellipodia-like protrusions toward the lateral H1 cells (Fig. 5 A). This study also revealed that lateral H2 cells produce a unique protrusion toward the dorsal cells (Fig. 5 B). To better characterize the morphology of the latter protrusion, we expressed a photoconvertible fluorescent protein, Kaede (Ando et al., 2002), in the hypodermis. Pulses of blue-light illumination of H2 lateral cells induced the photoconversion of Kaede GFPs into strong RFPs (Fig. 5 C). This spectral isolation of the H2 cell confirmed that it produces a unique, deep protrusion toward the dorsal cells, which displays a thin neck emerging from the cell body (Fig. 5, C and D, arrow) followed by a deep cytoplasmic extension (Fig. 5, C and D, arrowhead) in which was transferred part of the cytoplasm (Fig. 5 E; and Video 1). Such features were observed for amoeboid protrusions used by macrophage and invasive carcinoma to migrate (Carr et al., 2013). As observed in the latter cells (Wyckoff et al., 2006; Ma and Baumgartner, 2013), F-actin accumulated at the neck between the cell body of H2 and the protrusion as well as at the leading edge of the protrusion (Fig. 5 F). NMY-2::GFP also appeared to accumulate along the apical edge of this protrusion (Fig. 5 G).

In summary, these data suggest that dorsal cells produce large, flat lamellipodia-like protrusions toward the lateral cells, whereas H2 lateral cells produce deep amoeboid-like protrusions toward the dorsal cells. No protrusion was observed between lateral and ventral cells.

pix-1/pak-1 and *let-502* control the formation and shape of lamellipodia and amoeboid-like protrusions, respectively

We subsequently assessed whether *pix-1*, *pak-1*, and *let-502* control the protrusive activity of dorsal and lateral hypodermal cells. To do so, we measured the size of the protrusions produced by dorsal and lateral cells in wt embryos. Protrusions formed by dorsal cells spread along the longitudinal junction between dorsal 1/2 and lateral H1 cells. Therefore, we normalized the length of the protrusion on the length of this junction (see Materials and methods). The resulting spreading rate of the protrusions was significantly reduced in *pix-1(gk416)*, *pak-1(ok448)*, and *let-502(RNAi)* embryos compared with wt (Fig. 6, A and C). We also assessed the distribution of the protrusions along the longitudinal junction (see Materials and methods; Fig. S5). This revealed that protrusions disappeared specifically at the posterior part of this junction in *pix-1(gk614)* and *pak-1(ok448)* embryos (Fig. 6 D), suggesting that *pix-1* and *pak-1* control the formation and spreading of protrusions produced by dorsal cells specifically toward the posterior part of H1 lateral cells.

We characterized the protrusive activity of lateral cells by measuring the area covered by the protrusion on a *z*-stack projection (Fig. 7 A, white dashed line). This measurement revealed that the protrusion produced by H2 was significantly more spread in *let-502(RNAi)* embryos compared with wt and *pix-1(gk416)* embryos (Fig. 7, A and B). A slight but significant increase of the protrusion surface was also observed in *pak-1(ok448)* embryos. However, the latter surface increase did not correlate with the increase of spreading of the protrusion along the anteroposterior axis as observed for *let-502(RNAi)* animals (Fig. 7 A), suggesting that deletion of *pak-1* did not significantly change the morphology of the protrusion produced by the lateral cells. Interestingly, the surface of this protrusion was significantly reduced in *nmy-2(ne1490ts)* at 25°C compared with wt (Fig. 7, B and D). This suggests that myosin activity is required for the formation and spreading of this protrusion.

Altogether, these data suggest that *let-502* controls the morphology of the amoeboid-like protrusions produced by H2 cells, whereas *pix-1* and *pak-1* control the formation and the polarity of lamellipodia produced by dorsal cells. *let-502* may also control part of the protrusive activity of dorsal cells uniformly along the longitudinal junctions between dorsal and lateral cells. These data also show that myosin activity is required for the formation of the amoeboid protrusion produced by lateral cells. Altogether, these data suggest that *pix-1/pak-1* and *let-502* control the formation of convergent protrusions along the aligned D2/L2 junctions and that their functions are prominent in either dorsal or lateral cells. The fact that both protrusive activity and remodeling of apical junctions of lateral cells are dependent on LET-502 suggests that lateral cells adopted a LET-502 program to control molecular and cellular events involved in early elongation. Similar reasoning applies for dorsal cells and PIX-1/PAK-1. These data do not, however, establish whether protrusion formation and remodeling of apical junctions are functionally linked to one another or are parallel and independent processes.

pix-1 and *pak-1* functions contribute to the reduction of AJM-1::GFP anisotropy at D2/L2 vertex

D2 and L2 junctions display faster shrinking rates (Fig. 1 D) and more elevated myosin-dependent apical remodeling than D1 and L1 (Fig. 4, A and B), suggesting that the vertex located at the intersection of these junctions (D2/L2 vertex) is subjected to a higher tension than the D1/L1 vertex (Fig. 8, A and B). Considering that *pix-1/pak-1* and *let-502* control the formation of convergent protrusions along the aligned D2/L2 junctions, we assessed whether the formation of these protrusions may impact differently on the tension applied on D1/L1 and D2/L2 vertices. Consistent with the tension being higher at vertices compared with other locations of cell–cell junctions (black line; Fig. 8 C), AJM-1::GFP local anisotropy was significantly higher at D1/L1 and D2/L2 vertices when considering the junction between these vertices. AJM-1::GFP local anisotropy was also reduced at both vertices in a similar manner in *nmy(ne1490ts)* embryos at restrictive temperature (25°C) and in *let-502(RNAi)* embryos (Fig. 8, C and D, gray and green lines, respectively; *t* test, $P \leq 8 \times 10^{-5}$). AJM-1::GFP local anisotropy was reduced to a lower extent at D1/L1 vertex in *pak-1(ok448)* (Fig. 8, C and D, red line; *t* test, $P = 0.011$). Interestingly, the anisotropy was significantly increased only at D2/L2 in *pix-1(gk416)* (Fig. 8, C and D, blue line; *t* test, $P = 3 \times 10^{-5}$) and to a lower extent in *pak-1(ok448)* compared with wt (Fig. 8, C and D, red line; *t* test, $P = 0.016$). If we postulate that AJM-1::GFP anisotropy increases at the cell–cell junctions in response to increased tension applied on the junctions, these data suggest that NMY-2 and LET-502, and to a lesser extent PAK-1, increase the tension applied on both D1/L1 and D2/L2 vertices, which is consistent with their expected function on myosin contraction (Piekny et al., 2003; Gally et al., 2009). These data also suggest that the function of

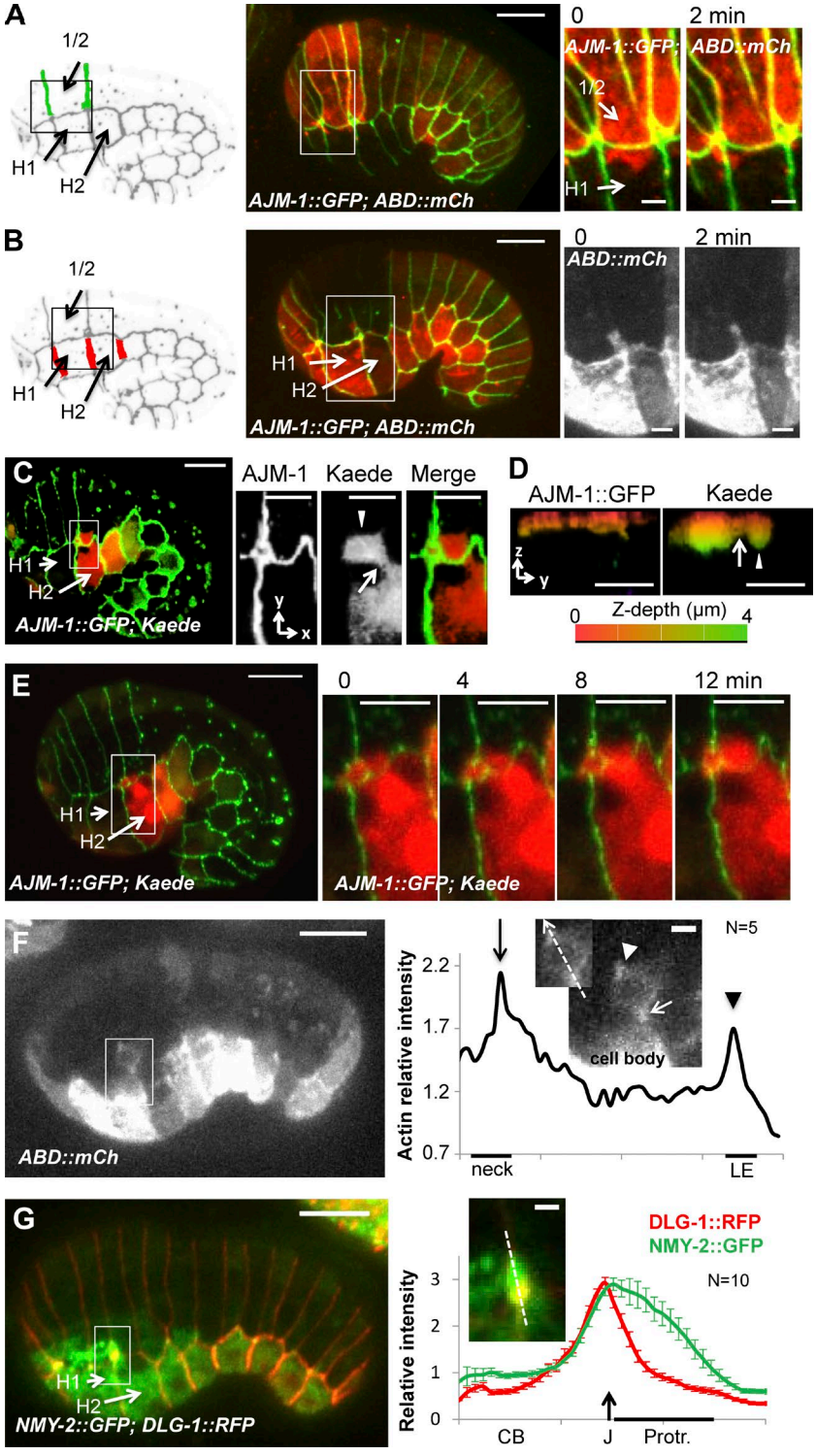

Figure 5. **Hypodermal cells produce convergent protrusions during early elongation.** Lamellipodia-like (A) and amoeboid-like (B) protrusions produced by dorsal and lateral cells, respectively, observed in embryos expressing AJM-1::GFP (green) and VAB-10(ABD)::mCherry (red). Locations of the enlarged images are indicated by a white box. *z*-projection (*xy* plane) (C) and *zy* plane (D) of an embryo expressing AJM-1::GFP (green) and Kaede (red) in hypodermal cells. Location of the enlarged images is indicated by a white box. The *z*-depth is represented by artificial color from the surface (0 µm; red) to 4-µm depth (green). The arrow and arrowhead indicate the cell body and the protrusion, respectively. (E) Time lapse recording of AJM-1::GFP (green) and Kaede (red). Bars: 10 µm; (enlarged images) 5 µm. (F) F-actin accumulation at the neck (arrow) and leading edge (LE; arrowhead) of amoeboid-like protrusion visualized in embryo expressing VAB-10(ABD)::mCherry and on the intensity plot along the dashed arrow indicated in the enlarged picture. (G) Myosin heavy-chain, NMY-2::GFP (green) accumulation observed at DLG-1/AJM-1 complex junction (J; arrow) in embryo expressing DLG-1::RFP (red) and on the intensity plot along the dashed arrow indicated in the enlarged picture. Cell body (CB) and the apical pole of amoeboid protrusion (Protr.) are indicated. Bars: 10 µm; (enlarged images) 2 µm. Data are representative of three independent experiments.

PIX-1 and, to a lesser extent, PAK-1 tends to decrease the tension applied on D2/L2 vertex. This hypothesis links mechanistically the regulation of apical remodeling that is dependent on myosin contraction and the formation of basolateral protrusions controlling the tension building at these junctions. Reduction of tugging forces applied on the D2/L2 vertex using laser-cutting of the L2 junction has been attempted to further test this hypothesis. Unfortunately, the embryo ruptures immediately after the junction is cut. Although appealing, this hypothesis remains consequently to be confirmed using an experimental system enabling the modulation of tugging forces applied to vertices without altering the molecular machines controlling the formation of protrusions or the integrity of the embryo.

Cell-autonomous antagonism between *let-502* and *pix-1/pak-1* controls the switch between Rac1- and RhoA-like morphogenetic programs

We subsequently assessed whether the cell-to-cell heterogeneity observed in hypodermis during early elongation depends on a

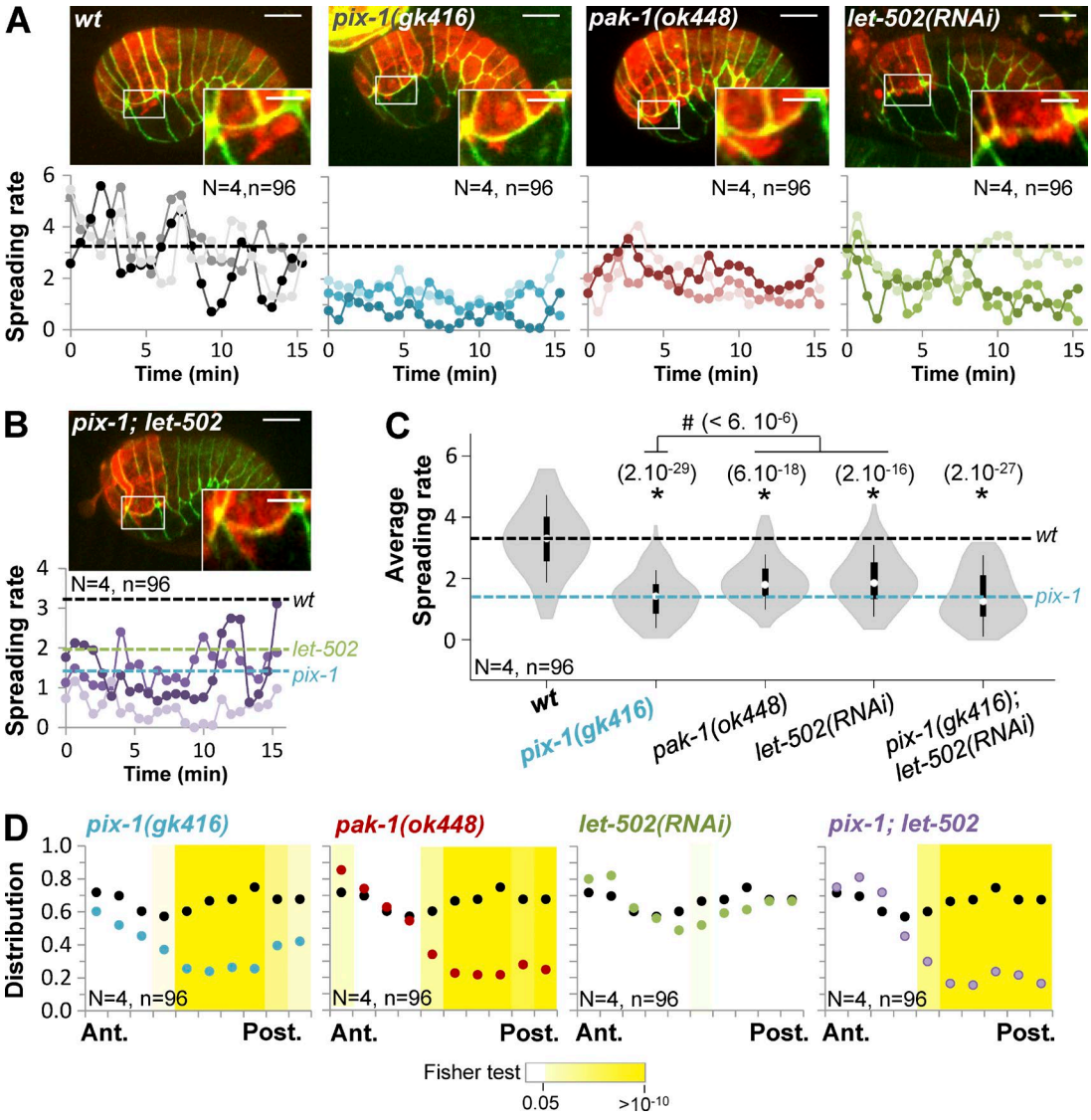

Figure 6. ***pix-1*and *pak-1* control the formation of polarized protrusions by dorsal anterior cells.** *z*-projections of confocal images and spreading rates of protrusions produced by dorsal cells are indicated over time (bottom) for three representative wt, *pix-1(gk416)*, *pak-1(ok448)*, and *let-502(RNAi)* (A) and *pix-1(gk416); let-502(RNAi)* (B) embryos expressing AJM-1::GFP (green; top) and VAB-10(ABD)::mCherry (red; top). Bars: 10 µm; (enlarged images) 5 µm. The dashed lines correspond to mean spreading rates for wt (black), *pix-1(gk416)* (blue), and *let-502(RNAi)* (green). (C) Violin plot representing the distribution and mean spreading rates for *N* = 4 embryos and *n* = 96 measurements. *t* test p-values significantly different from wt (*) and *pix-1(gk416)* (#) are indicated in parentheses. (D) Anteroposterior distribution of protrusions produced by dorsal cells. The black line corresponds to the distribution observed in wt embryos. p-values of Fisher exact test are indicated.

cell-autonomous antagonism between the Rac1 and RhoA pathways, as shown for isogenic populations of mesenchymal cells in vitro (Sailem et al., 2014). To do so, we assessed whether knockout of *pix-1* or *pak-1* induces a switch of the morphogenetic program adopted by dorsal cells toward *let-502*. Therefore, we measured the anisotropy of AJM-1::GFP at D1 and D2 junctions between dorsal cells in *pix-1(gk416); let-502(RNAi)* and *pak-1(ok448); let-502(RNAi)*. This analysis revealed that *let-502(RNAi); pix-1(gk416)* displayed significantly lower AJM-1::GFP anisotropy at D2 than *pix-1(gk416)* embryos (*t* test, P = 0.019; Fig. 9 A). Similar, although less significant, results were obtained when comparing *pak-1(ok448); let-502(RNAi)* and *pak-1(ok448)* (*t* test, P = 0.046; Fig. 9 A). No significant difference was observed for D1. These data suggest that *let-502* controls the remodeling of D2 apical junctions in the absence of *pix-1* and to a lesser extent in the absence of *pak-1*.

Similarly, we assessed whether the knockdown of *let-502* may switch lateral cells from a RhoA- to a Rac1-like program. To do so, we measured AJM-1::GFP anisotropy at L1 and L2 junctions in *pix-1(gk416); let-502(RNAi)* and *pak-1(ok448); let-502(RNAi)*. This analysis revealed that *pak-1(ok448)*, but not *pix-1(gk416)*, slightly but significantly reduced AJM-1::GFP anisotropy at L2 junction of *let-502(RNAi)* embryos (*t* test, P = 0.03; Fig. 9 B). No significant difference was observed for these mutants at L1. This suggests that *pak-1* has a significant function in the remodeling of L2 but not L1 apical junctions upon *let-502* knockdown.

To better understand the mechanisms underlying this switch between RhoA- and Rac1-like programs, we further characterized the structure of apical junctions through measurement of AJM-1::GFP cluster density (see Materials and methods; Fig. 9 C). This revealed that L2 displayed a significant

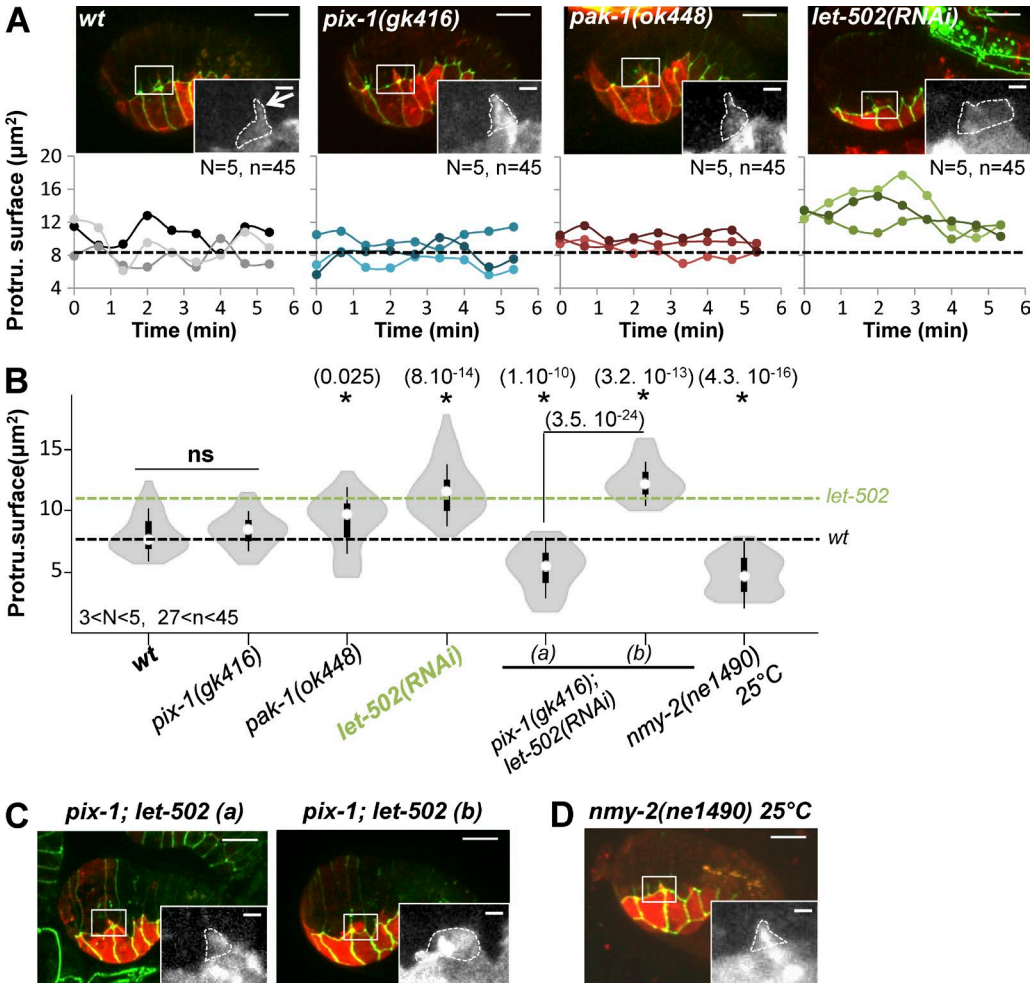

Figure 7. ***let-502* controls the formation of protrusions by lateral anterior cells.** (A) *z*-projections of confocal images and protrusion surface over time (bottom) are indicated for three representative wt, *pix-1(gk416)*, *pak-1(ok448)*, and *let-502(RNAi)* embryos expressing AJM-1::GFP (green; top) and VAB-10(ABD)::mCherry (red; top). The dashed lines correspond to the mean spreading rates for wt (black; A and B) and *let-502(RNAi)* (green; B). (B) Violin plot representing the distribution and mean of the protrusion surfaces for *N* analyzed embryos and *n* analyzed protrusions. *z*-projections of confocal images of populations (a) and *pix-1(gk416); let-502(RNAi)* embryos (b). *N* > 3 embryos were analyzed per genotype and junction (C) of *nmy-2(ne1490)ts* animals at 25°C (D). Significant *t* test vs. wt; p-values (*) are indicated in parentheses. ns, not significant. Bars: 10 µm; (enlarged images) 2 µm.

increase of AJM-1 cluster density in *let-502(RNAi)* compared with wt, *pix-1(gk416)*, and *pak-1(ok448)* (*t* test vs. wt, P = 0.001; Fig. 9, C and D). This increase was maintained in *pak-1(ok448); let-502(RNAi)* and completely suppressed at L2 junctions in *pix-1(gk416); let-502(RNAi)* embryos (*t* test vs. *let-502*, P = 0.004; Fig. 9 C). Similar trends, but no significant effects, were observed at L1 junctions. Because identification of protein clusters at cell–cell junctions requires high accumulation levels of these proteins, this analysis could not be done for junctions between dorsal cells.

Together, these data suggest that lateral hypodermal cells switch from a RhoA-like program to a Rac1-like program involving *pix-1* and *pak-1* upon functional alteration of *let-502*. In these conditions, *pix-1* controls AJM-1 cluster density and *pak-1* controls the AJM-1::GFP anisotropy at L2 junctions between lateral cells. These data also suggest that in the absence of *let-502*, *pix-1* and *pak-1* control the remodeling of L2 but not L1 junctions.

These data suggest that the adoption of a RhoA-like program by lateral cells depends on the inhibition of *pix-1* and *pak-1* by *let-502*. *let-502* is expected to control early elongation mainly through activation of myosin contraction at the apical junctions of hypodermal cells (Piekny et al., 2000). The function of *pix-1* and its homolog β-PIX were shown in both *C. elegans* and mammals to be regulated by mechanical stimuli (Zhang et al., 2011; Plutoni et al., 2016). We consequently assessed whether LET-502 may indirectly inhibit PIX-1 through its function on myosin contraction. To test this possibility, we measured AJM-1 cluster density at L2 junctions in *nmy-2(ne1490ts)* embryos at permissive (18°C) and restrictive (25°C) temperatures (Fig. 9, B–D). No significant difference of AJM-1::GFP cluster density was observed in these conditions compared with wt animals, suggesting that LET-502 inhibits PIX-1 in lateral cells, independently from its function on NMY-2.

We also assessed whether the switch between morphogenetic programs controlling apical junction remodeling is associated with a change of protrusion morphology. The spreading rate and the anteroposterior distribution of the protrusions produced by dorsal cells in *let-502(RNAi); pix-1(gk416)* were similar to those measured in *pix-1(gk416)* embryos (Fig. 6, B and C), suggesting that *let-502* does not control the formation and polarity of protrusions produced by these cells in the absence of

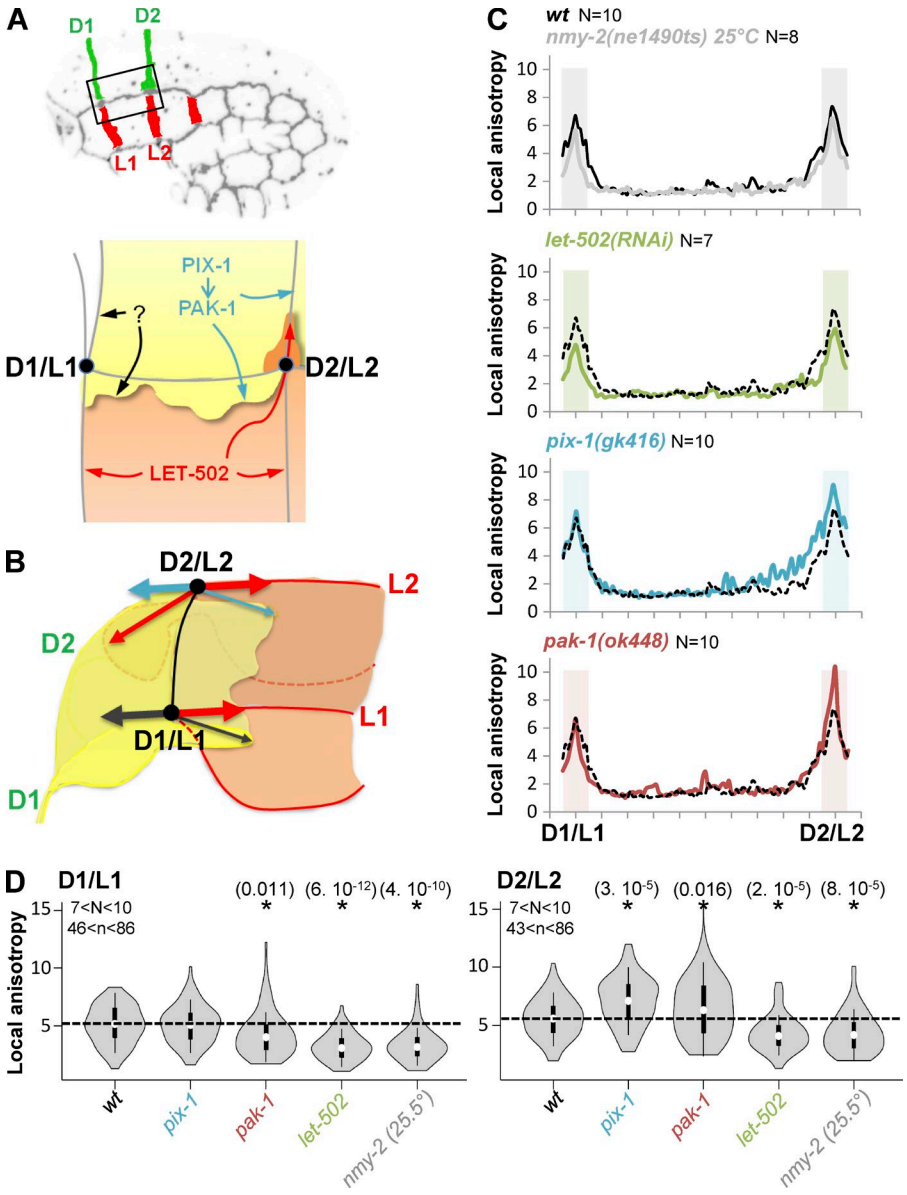

Figure 8. **AJM-1::GFP local anisotropy at D2/L2 vertex is increased in *pix-1* and *pak-1* mutants.** (A and B) Schematic representation of lateral and dorsal anterior cells, identifying cell–cell junctions as well as the function shown for *let-502*, *pix-1*, and *pak-1* on apical junction remodeling and formation of basolateral protrusions. D1/L1 and D2/L2 vertices are also indicated. Arrows represent direction of forces produced by machineries remodeling apical junction and basolateral protrusions. (C) Local anisotropy of AJM::GFP along the longitudinal junction between D1/L1 and D2/L2 vertices in wt (black line), *nmy-2(ne1490ts)* at restrictive temperature 25°C, *let-502(RNAi)*, *pix-1(gk416)*, and *pak-1(ok448)*. Areas of the junctions submitted to Student's *t* test for mutants vs. wt are shaded. $N > 7$ embryos were analyzed per genotype and junction. (D) Violin plot representing the distribution and mean local anisotropy of AJM-1::GFP for *N* analyzed embryos and *n* analyzed junctions. *, Significant *t* test vs. wt. P-values are indicated in parentheses.

pix-1. However, the overspread protrusion produced by the lateral H2 cell in *let-502(RNAi)* animals was inhibited in more than 50% ($n = 10$) of *pix-1(gk416); let-502(RNAi)* embryos (Fig. 7, B and C). These data suggest that *pix-1* controls the morphology of protrusions produced by lateral cells in *let-502(RNAi)* embryos. The low penetrance of this inhibition by *pix-1(gk416)* also suggests that *pix-1* controls the morphology of these protrusions, in parallel with genes that remain to be identified. Unfortunately, the level of F-actin detected by the VAB-10(ABD)::mCherry probe in *pak-1(ok4480); let-502(RNAi)* embryos was too low to assess the morphology and spreading of protrusions produced by dorsal and lateral cells in these animals. Altogether, these data suggest that PIX-1 controls the formation of protrusions at lateral cells in the absence of LET-502, but that LET-502 does not control the formation of protrusion by dorsal cells in the absence of PIX-1. To explain these results, we may hypothesize that LET-502 is not active enough in dorsal cells, even in the absence of PIX-1, to promote the formation of amoeboid protrusions, or that LET-502 is missing some functionality to enable the formation of polarized protrusions in these cells.

Discussion

Antagonism between Rac1 and RhoA has been shown to control different morphogenetic processes during embryonic development, the activation of these GTPases being restricted to mutually exclusive subcellular or sequential compartments (Duan et al., 2010; Chauhan et al., 2011). We used a quantitative imaging approach to characterize the function of the RhoA-like *rho-1/let-502* and the Rac1-like *pix-1/pak-1* pathways at the single-cell level during early elongation in *C. elegans*. This study revealed that *pix-1* and *pak-1* are mainly involved in the remodeling of apical junctions between dorsal and ventral anterior cells, whereas *let-502* controls the remodeling of apical junctions between lateral cells and between ventral posterior cells. This study also revealed that dorsal and lateral anterior cells produce basolateral protrusions in a polarized and convergent manner: dorsal cells produce flat lamellipodia-like protrusions toward the lateral cells, and lateral cells produce deep amoeboid-like protrusions toward the dorsal cells. Intriguingly, this study also

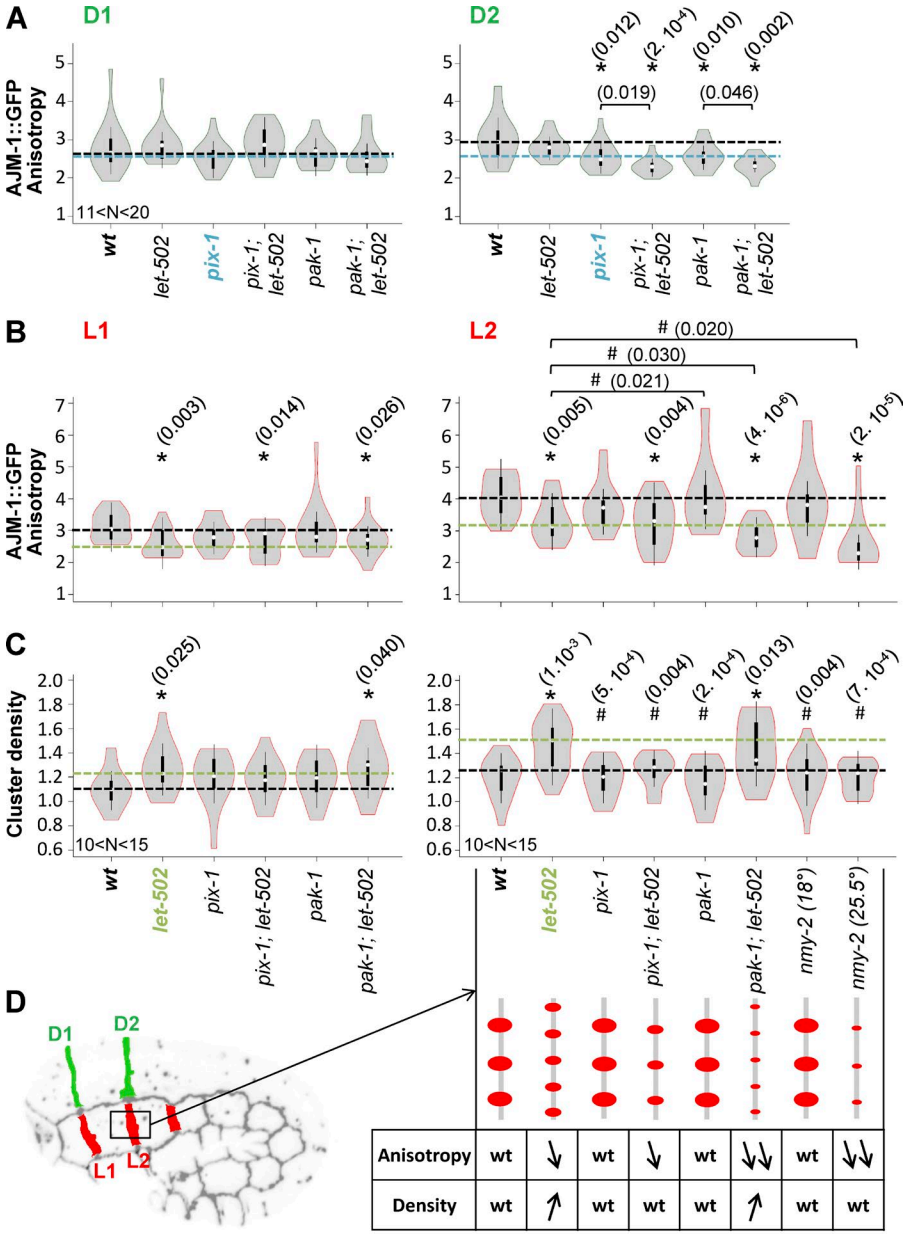

Figure 9. **PIX-1/PAK-1 and LET-502 are antagonistic in dorsal and lateral anterior cells.** Violin plot representing the distribution and mean AJM-1::GFP anisotropy measured at dorsal anterior D1 and D2 junctions (A) and lateral anterior L1 and L2 junctions (B) in wt, *let-502(RNAi)*, *pix-1(gk416)*, *pix-1(gk416); let-502(RNAi)*, *pak-1(gk416)*, and *pak-1(gk416);let-502(RNAi)* embryos expressing AJM-1::GFP and VAB-10(ABD)::mCherry as well as *nmy-2(ne1490ts); ajm-1::GFP* at 18°C or 25°C. (C) Density of AJM-1::GFP clusters measured for the lateral anterior L1 and L2 junctions. The dashed lines indicate the mean value for wt (black), *pix-1(gk416)* (blue), and *let-502(RNAi)* (green). (D) Schematic representation of cluster density and anisotropy for each strain. $N > 10$ embryos were analyzed per genotype and junction. *t* test p-values significantly different from wt (*) and *let-502(RNAi)* (#) are indicated in parentheses.

suggests that *pix-1/pak-1*–dependent protrusions produced by dorsal cells may reduce the tension building between dorsal and lateral cells during early elongation. Because tension building at apical junctions is associated with the remodeling of these junctions, the latter hypothesis may mechanistically link the formation of basolateral protrusions by a cell and the remodeling of its apical junctions. Importantly, this study proposes that adoption by the cells of either a *pix-1/pak-1* (Rac1-like) or a *let-502* (RhoA-like) program defines their morphology and behavior during morphogenesis (Fig. 10). Therefore, cell-autonomous antagonism between *pix-1/pak-1* and *let-502* defines cell-to-cell heterogeneity during epidermal morphogenesis, enabling cells to switch between programs when one of these genes gets genetically compromised (Fig. 10, B and C). *pix-1/pak-1* and *let-502* pathways, while being antagonistic at a single-cell level, function in a synergistic manner when considered at the organism level, presumably as a result of the cooperation of cells during elongation.

Remodeling of apical junctions uses either LET-502 or PIX-1/PAK-1

Results obtained here are in agreement with previous studies showing that PIX-1 and PAK-1 control early elongation in parallel with LET-502 (Gally et al., 2009; Martin et al., 2014) and predominantly function at the anterior part of the embryo (Martin et al., 2014). During *D. melanogaster* development, DPAK/PAK-1 was shown to control salivary gland lumen size through modulation of myosin-dependent endocytic processes (Pirraglia et al., 2010). A similar function was also reported for ROK/LET-502 during germ-band extension in that organism (Bertet et al., 2004). Remodeling of apical junctions through the regulation of myosin-dependent endocytosis by PIX-1/PAK-1 or LET-502 is an attractive hypothesis that will provide a mechanistic link between apical junction remodeling and junction shrinking. It still needs to be tested during early elongation in *C. elegans*.

This study also revealed that although both PIX-1 and PAK-1 control the anisotropy of AJM-1::GFP at the apical junctions between dorsal cells, they tend to display distinct

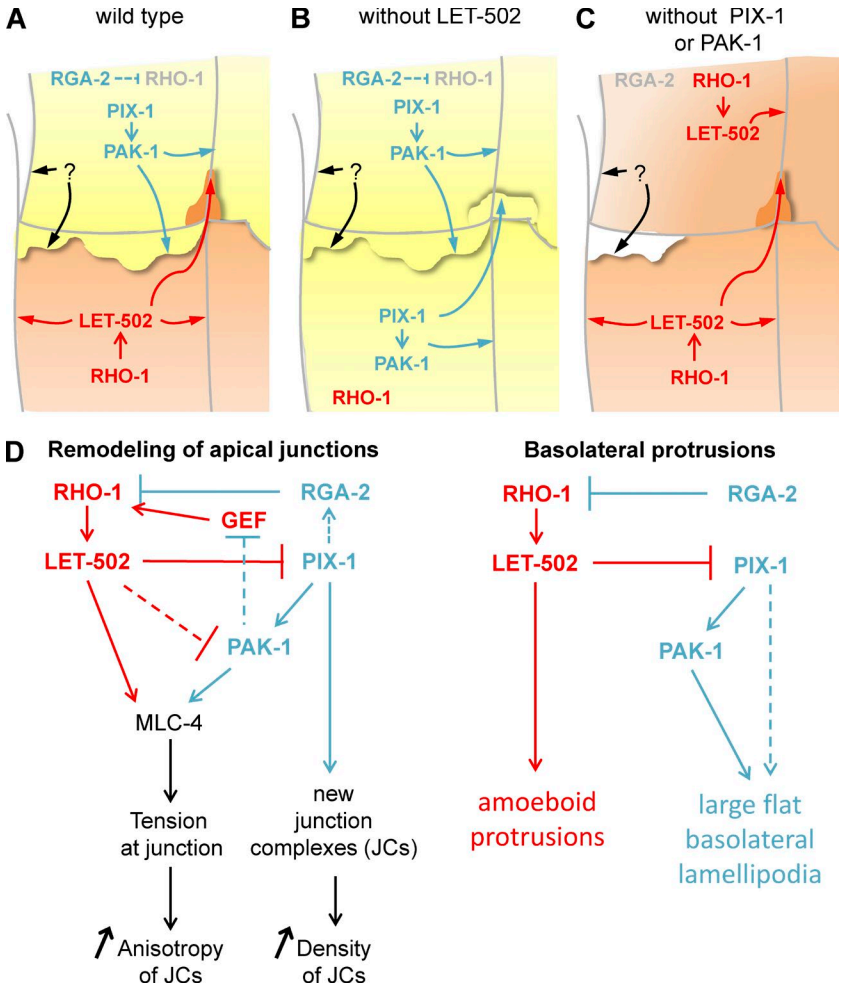

Figure 10. **Model for Rho/Rac-like antagonism during early elongation.** (A–C) Schematic representation of signaling pathways controlling morphogenesis in dorsal and lateral cells in wt embryos (A), *let-502* knockdown or mutants (B), and *pix-1* or *pak-1* mutants (C). Cells after a Rac1-like morphogenetic program involving PIX-1 and PAK-1 are represented in yellow, and those after a RhoA-like program involving RHO-1 and LET-502 are represented by orange. (D) Effect of Rac1/RhoA antagonism on remodeling of apical junction (left) and formation of basolateral protrusions (right).

molecular functions at the apical junctions between lateral cells in the absence of LET-502. For instance, in the latter conditions, PAK-1 controls AJM-1::GFP anisotropy at apical junctions, whereas PIX-1 controls AJM-1::GFP cluster density (Fig. 10). That PIX-1 and PAK-1 may have common and independent functions during morphogenesis has already been suggested (Martin et al., 2014). We cannot exclude the possibility, however, that PIX-1 and PAK-1 may function redundantly with genes that remain to be identified in lateral cells.

Basolateral protrusions may reduce the tension building at cell–cell junctions during morphogenesis

Basolateral protrusions produced by epithelial cells during morphogenesis have been described as motor structures enabling directional cell movement (Heid et al., 2001; Farooqui and Fenteany, 2005; Zallen, 2007). The protrusions produced by dorsal and lateral cells during early elongation, identified here, are not associated with any notable relative displacement of these cells within the epithelium. Although the function of these protrusions is still unclear, this study suggests that formation of *pix-1*– and *pak-1*–dependent lamella may reduce the tension applied on the D2/L2 vertex (Fig. 8). Such a hypothesis is in agreement with recent studies showing that forces applied on cell–cell junctions are counterbalanced by traction forces produced by protrusions and biased away from this interface (Liu et al., 2010; Maruthamuthu et al., 2011; Weber et al., 2012). We hypothesize that PIX-1/PAK-1–dependent lamellae generate traction forces at the D2/L2 vertex in the opposite direction from that of forces produced by the PIX-1/PAK-1 pathway controlling D2 shrinking. Forces produces by these protrusions may consequently reduce the tugging forces applied to this vertex (Fig. 8 B). Note that all data obtained in this study involving protrusion formation revealed a prominent role played by PIX-1 over PAK-1, suggesting that PAK-1 may function in parallel to a gene that remains to be identified downstream of PIX-1 (Fig. 10 D). Supporting the involvement of PIX-1 in this process, β-PIX/PIX-1 has been identified as a mechanotransducer in both mammals and *C. elegans* (Kuo et al., 2011; Vicente-Manzanares et al., 2011; Zhang et al., 2011; Plutoni et al., 2016).

No experimental evidence helped us to assess the function of the amoeboid-like protrusions produced by lateral cells. The location of this protrusion along the D2/L2 transversal junction, which is supposed to be subjected to the highest level of myosin contraction, is intriguing, however, because amoeboid protrusions were shown to form at a region where the membrane is weakly attached to the cortex as a result of changes in cortical myosin contractions (Charras et al., 2005).

Antagonism between RhoA-like and Rac1-like programs define cell-to-cell heterogeneity during epidermal morphogenesis

Mutual inhibition between Rac1 and RhoA allows the cell to switch between biochemical processes associated with different

cellular phenotypes (Jilkine et al., 2007; Symons and Segall, 2009; Tsyganov et al., 2012). It also allows the cell to make a discrete decision when exposed to environmental fluctuation while ensuring robustness of cellular behavior (Byrne et al., 2016). Antagonism between Rac1 and RhoA allows the mutually exclusive activation of these GTPases during cell migration and organogenesis (Jilkine et al., 2007; Pertz, 2010; Guilluy et al., 2011; Semplice et al., 2012). Interestingly, in carcinoma cells, the mutual inhibition of Rac1 and RhoA controls the morphological switch enabling cells to use either lamellae-driven (Rac1 program) or amoeboid-driven (RhoA program) migration (Ohta et al., 2006; Saito et al., 2012; Nakamura, 2013). Altogether, these studies are consistent with data reported here showing that cells produce either lamellipodia-like protrusions in a PIX-1/PAK-1–dependent manner or amoeboid-like protrusions in a LET-502–dependent manner.

Several mechanisms involving regulators and effectors of RhoA and Rac1 have been involved in the mutual inhibition of these GTPases, as reviewed by Guilluy et al. (2011). Data presented here suggest that PIX-1, PAK-1, and LET-502 control Rac1/RhoA antagonism during embryonic elongation. In the absence of PIX-1 or PAK-1, LET-502 partially restores apical junction remodeling between dorsal cells. The partial compensation provided by LET-502 in these conditions suggests that PIX-1 and PAK-1 may only partially contribute to the inhibition of LET-502 function in dorsal cells. The current study also suggests that LET-502 inhibits PIX-1 and PAK-1 in the lateral cells during early elongation. ROCK/LET-502 and β-PIX/PIX-1 have been shown to be involved in RhoA-dependent inactivation of Rac1 in mammalian cells, ROCK function displacing β-PIX from focal adhesion complex during junction maturation (Kuo et al., 2011; Vicente-Manzanares et al., 2011).

Collectively, these data suggest that epithelial cells can adopt either RhoA or Rac1 morphogenetic programs that are associated with morphologically distinctive properties despite being fully polarized, cohesive, and cooperative during morphogenesis. These are quite novel and provocative results that could explain the evolutionarily conserved cell-shape heterogeneity observed in animal and plant epithelia. This study also suggests that morphogenetic processes should be characterized at a single-cell level, to assess whether cell-to-cell heterogeneity during epithelial morphogenesis is a specific characteristic of *C. elegans* hypodermis or an evolutionarily conserved characteristic of epithelial cell type.

Materials and methods

Strains and culture methods

Control N2 (wt) and other animals were maintained using standard culture conditions at 20°C (Brenner, 1974). Worm strains carried the following mutations and markers. *pix-1(gk416) X* (VC863), *pak-1(ok448) X* (RB689), *jcIs1 [ajm-1::GFP + unc-29(+) + rol-6(su1006)] IV* (SU93), *mcIs40 [lin-26p::ABDvab-10::mCherry + myo-2p::GFP]* (ML916), and *unc-119(ed3)* were obtained from the Caenorhabditis Genetic Center. Mutant strains were backcrossed at least three times against wt animals before analysis. Strains carrying *let-502(sb118) I; jcIs1 [ajm-1::GFP + unc-29(+) + rol-6(su1006)] IV*, *nmy-2(ne1490ts); jcIs1 [ajm-1::GFP + unc-29(+) + rol-6(su1006)] IV*, and *cp7 [nmy-2::GFP + LoxP unc-119(+) LoxP]; mcIs46 [dlg-1::RFP + unc-119]* were provided by A. Piekny (Concordia University, Montreal, QC, Canada). *jcIs1 [ajm-1::GFP + unc-29(+) + rol-6(su1006)] IV*; *mcIs40 [lin-26p::ABDvab-10::mcherry + myo-2p::GFP]* was generated after crossing ML916 males with SU93 hermaphrodites. *pix-1(gk416) X*, *jcIs1 [ajm-1::GFP + unc-29(+) + rol-6(su1006)] IV*; *mcIs40 [lin-26p::ABDvab-10::mcherry + myo-2p::GFP]*, and *pak-1(ok448) X; jcIs1 [ajm-1::GFP + unc-29(+) + rol-6(su1006)] IV*; *mcIs40 [lin-26p::ABDvab-10::mcherry + myo-2p::GFP]* were generated after crossing *jcIs1 [ajm-1::GFP + unc-29(+) + rol-6(su1006)] IV; mcIs40 [lin-26p::ABDvab-10::mcherry + myo-2p::GFP]* hermaphrodites with *pix-1(gk416) X* or *pak-1(ok448) X* males. *unc-119(ed3); jcIs1 [ajm-1::GFP + unc-29(+) + rol-6(su1006)] IV* was generated by crossing *unc-119(ed3)* hermaphrodites with *jcIs1 [ajm-1::GFP + unc-29(+) + rol-6(su1006)] IV* males.

Generation of transgenic animals

unc-119(ed3); sajIs50 [lin-26p::KAEDE + unc-119^R] animals were generated by biolistic bombardment. The expression vector used to generate this transgene was made using MultiSite Gateway technology (Invitrogen). pCG150 destination vector (Addgene) was recombined with a pDONRP4P1R vector containing 5 kb of the *lin-26* promoter (*lin-26p*; Martin et al., 2014), a pDONR201 containing the coding sequence for *KAEDE* protein amplified from Kaede-N1 (Addgene), and a pCM5.37 containing the *unc-54* 3′UTR (Addgene). This construct was used to generate transgenic animals by biolistic bombardment of *unc-119(ed3)* strain, using a PDS-1000/He system with the Hepta adaptor (Bio-Rad Laboratories) with the following parameters: 4-mm distance between the exits of the Hepta adaptor gas splitter and macrocarriers, 20-mm distance between stopping screens and target shelf, 1,350-psi rupture disks, and vacuum at 28 inches of mercury (Berezikov et al., 2004). Transgenic animals expressing AJM-1::GFP together with KAEDE were obtained through crossing *unc-119(ed3)*; *jcIs1 [ajm-1::GFP + unc-29(+) + rol-6(su1006)] IV* hermaphrodites with *unc-119(ed3); sajIs50 [lin-26p::KAEDE + unc-119^R]* males.

RNA interference treatment

pL4440 constructs containing the *let-502* coding sequence were retrieved from the genome-wide library (Kamath and Ahringer, 2003) and confirmed by sequencing. HT115 bacteria transformed with pL4440 vectors were plated on LB medium with ampicillin (30 µg/ml) and tetracycline (30 µg/ml) and grown overnight at 37°C. The next day, isolated colonies of HT115 clones were picked and grown overnight in LB ampicillin (30 µg/ml). RNAi expression was induced by IPTG (30 µg/ml) for 1 h at 37°C. 700 µl bacterial culture was pelleted and resuspended in 300 µl S-basal medium with ampicillin (30 µg/ml) and IPTG (30 µg/ml) and put in a 24-well plate. 150–200 L1 worms synchronized through hypochlorite treatment were resuspended in 200 µl S-basal medium and incubated with 300 µl induced bacteria at 20°C for 48–60 h before microscopy analysis.

Measurement of cell–cell junction deformation

Images used to measure membrane deformation were captured using an A1R confocal microscope (Nikon) equipped with 60× oil CFI NA 1.4 Plan Apochromat λ objective. 60 *z*-planes (top and bottom defined to record throughout the entire embryo) were acquired per embryo with a calibration of 0.12 µm/pixel and a *z*-step of 0.4 µm. *z*-stacks were captured at the beginning of the early elongation (t_0) and after 15 to 20 min, making sure that the last recording was done before the beginning of late elongation, the time point when body wall muscles start to contract. Deformation of cell–cell junctions was measured using Vaa3D software (Peng et al., 2010). To do so, *z*-stack acquisitions were resampled using a factor of 0.3 to obtain cubic voxels (0.12 × 0.12 × 0.12 µm), enabling accurate measurement of cell–cell junctions using the 3D reconstruction of image stacks. Cell–cell junction lengths at t_0 (L_0) and

after 15 to 20 min (L_{end}) were measured (in pixels) between each vertex identified in the 3D reconstruction. The deformation (D) of a junction x in a mutant m was computed as follows: $D_{x/m} = (L_{end} - L_0)/(t_{end} - t_0)$. With $D_{x/wt}$ being the deformation of the junction x in wt embryos, we calculated the relative deformation rate (RDR) of junction x in the mutant m as follows: if both $D_{x/wt}$ and $D_{x/m}$ are positive or negative: $RDR_{x/m} = |\log(D_{x/m}/D_{x/wt})|$. If ($D_{x/wt} > 0$ and $D_{x/m} < 0$) or ($D_{x/wt} < 0$ and $D_{x/m} > 0$): $RDR_{x/m} = |\log(|D_{x/m} - D_{x/wt}|/|D_{x/wt}|)|$. RDR is assigned a negative value if junction x is shorter in m than in wt and a positive value otherwise. Note that all junctions could not be measured for each embryo because of their orientation; however, a minimum of five embryos was used to measure the deformation of each cell–cell junction for this study.

Measurement of AJM-1::GFP anisotropy

Acquisitions recorded for membrane deformation were also used to measure AJM-1::GFP anisotropy. ImageJ software was used to generate a z-projection of 15–20 upper stacks. Fluorescence intensity plot profiles were drawn for each cell–cell junction between vertices using the segmented line tool. The minimum (I_{min}) and maximum (I_{max}) intensity were thus extracted from these profiles for each junction, and the anisotropy (A) of AJM-1::GFP accumulated at this junction was computed as previously reported (Engl et al., 2014), using $A = I_{max}/I_{min}$.

The local anisotropy ($LA(x)$) at a given location x along the cell–cell junction considers the fluorescence intensity of AJM-1::GFP at position x (I_x) and the minimum intensity (I_{min}) measured for this junction as follows: $LA(x) = I_x/I_{min}$.

Measurement of protrusion surface, spreading, and polarity

Image acquisitions to measure protrusion formation by hypodermal cells were done on wt and mutant animals expressing *jcIs1[ajm-1::GFP + unc-29(+) + rol-6(su1006)] IV; mcIs40[lin-26p::ABDvab-10::mCherry + myo-2p::GFP]* embryos using both Nikon A1R confocal and swept-field confocal microscopes with a 100× oil CFI NA 1.45 Plan Apochromat λ objective. The Nikon A1R confocal was used to photobleach F-actin binding probe in cells surrounding the cell of interest. Photobleaching used several stimulations at 100% power efficiency of 488- and 561-nm laser. F-actin binding probe and AJM-1::GFP were then recorded in unbleached cells using the swept-field confocal microscope by capturing 15 z-planes with 0.400-µm z-intervals every 40 s for 7 min (for protrusions produced by the lateral cells toward the dorsal cells) or 20 min (for protrusions produced by dorsal and ventral cells toward the lateral cells). The length of the protrusions formed by the dorsal cells was measured using ImageJ software, as well as the length of the cell–cell junction between D1/L1 and D2/L2 vertices. The spreading rate of the protrusions produced by dorsal cells was then calculated as the length of protrusions versus the length of the measured cell–cell junctions. Considering the peculiar morphology of the amoeboid-like protrusion produced by the lateral cells, we measured the surface covered by this protrusion on a z-projection of the image stack as shown in Fig. 7. The spreading rate of the protrusion produced by dorsal cells was measured at 24 time points per embryo for four different embryos. The surface of protrusions produced by lateral cells was measured at nine time points per embryo for five different embryos.

To measure the polarity/distribution of the protrusions produced by the dorsal cells, we divided the cell–cell junction located between the D1/L1 and D2/L2 vertices into 10 equal sections. We identified the presence of the protrusion at each section at 24 different time points for four different embryos. We subsequently computed the distribution as the percentage of positive events per measurement per section as indicated in Fig. S5.

Statistical analyses

Two-tailed Student t test computed using Excel tools was used to assess the statistical significance of differences observed between populations of measurements done on embryos with different genotypes. Normal distributions of our data were assessed using Lilliefors test (http://in-silico.net/tools/statistics/lillieforstest). Fisher's exact test (computed using R statistical tools, Bioconductor) was used in Fig. 6 D to assess the significance of the reduction or of the increase of the number of protrusions observed at a given section along the cell–cell junction between dorsal 1/2 and lateral H1 cells for a given mutant compared with wt embryos. Spearman correlation coefficients and associated p-values were computed using R statistical tools (Bioconductor).

Online supplemental material

Fig. S1 shows that *ajm-1::GFP; vab-10(ABD)::mCherry*–carrying embryos develop as wt animals. Fig. S2 shows the step-by-step method to quantify junction elongation rates. Fig. S3 shows the deformation rate of transversal L2 junctions measured for four different wt embryos. Fig. S4 shows that *let-502(RNAi)*–treated animals display defects similar to those of *let-502(sb118ts)* mutants grown at nonpermissive temperature. Fig. S5 shows the method used to quantify the distribution of protrusions along the junction between D1/L1 and D2/L2 vertices. Video 1 shows the transfer of H2 cytoplasm to the amoeboid protrusion.

Acknowledgments

Thanks to Dr. Alisa Piekny, Dr. Claire Benard (Université du Québec à Montréal, Montréal, Canada), and Dr. Christelle Gally (Institut Génétique Biologie Moléculaire Cellulaire, Illkirch, France) for sharing biological materials and critical comments on the manuscript. Some of the strains were provided by the Caenorhabditis Genetics Center, which is funded by the National Institutes of Health Office of Research Infrastructure Programs (P40 OD010440).

The research was funded by the Natural Sciences and Engineering Research Council of Canada. E. Martin and M.-H. Ouellette were funded by Université du Québec à Montréal, Fellows Award for Research Excellence (FARE) fellowships.

The authors declare no competing financial interests.

Submitted: 5 April 2016
Revised: 29 July 2016
Accepted: 19 October 2016

References

Ando, R., H. Hama, M. Yamamoto-Hino, H. Mizuno, and A. Miyawaki. 2002. An optical marker based on the UV-induced green-to-red photoconversion of a fluorescent protein. *Proc. Natl. Acad. Sci. USA.* 99:12651–12656. http://dx.doi.org/10.1073/pnas.202320599

Berezikov, E., C.I. Bargmann, and R.H. Plasterk. 2004. Homologous gene targeting in *Caenorhabditis elegans* by biolistic transformation. *Nucleic Acids Res.* 32:e40. http://dx.doi.org/10.1093/nar/gnh033

Bertet, C., L. Sulak, and T. Lecuit. 2004. Myosin-dependent junction remodelling controls planar cell intercalation and axis elongation. *Nature.* 429:667–671. http://dx.doi.org/10.1038/nature02590

Brenner, S. 1974. The genetics of *Caenorhabditis elegans*. *Genetics.* 77:71–94.

Byrne, K.M.M., N. Monsefi, J.C. Dawson, A. Degasperi, J.C. Bukowski-Wills, N. Volinsky, M. Dobrzyński, M.R. Birtwistle, M.A. Tsyganov, A. Kiyatkin, et al. 2016. Bistability in the Rac1, PAK, and RhoA signaling network drives actin cytoskeleton dynamics and cell motility switches. *Cell Syst.* 2:38–48. http://dx.doi.org/10.1016/j.cels.2016.01.003

Carr, H.S., Y. Zuo, W. Oh, and J.A. Frost. 2013. Regulation of focal adhesion kinase activation, breast cancer cell motility, and amoeboid invasion by the RhoA guanine nucleotide exchange factor Net1. *Mol. Cell. Biol.* 33:2773–2786. http://dx.doi.org/10.1128/MCB.00175-13

Charras, G.T., J.C. Yarrow, M.A. Horton, L. Mahadevan, and T.J. Mitchison. 2005. Non-equilibration of hydrostatic pressure in blebbing cells. *Nature.* 435:365–369. http://dx.doi.org/10.1038/nature03550

Chauhan, B.K., M. Lou, Y. Zheng, and R.A. Lang. 2011. Balanced Rac1 and RhoA activities regulate cell shape and drive invagination morphogenesis in epithelia. *Proc. Natl. Acad. Sci. USA.* 108:18289–18294. http://dx.doi.org/10.1073/pnas.1108993108

Collinet, C., M. Rauzi, P.F. Lenne, and T. Lecuit. 2015. Local and tissue-scale forces drive oriented junction growth during tissue extension. *Nat. Cell Biol.* 17:1247–1258. http://dx.doi.org/10.1038/ncb3226

Costa, M., W. Raich, C. Agbunag, B. Leung, J. Hardin, and J.R. Priess. 1998. A putative catenin-cadherin system mediates morphogenesis of the *Caenorhabditis elegans* embryo. *J. Cell Biol.* 141:297–308. http://dx.doi.org/10.1083/jcb.141.1.297

Diogon, M., F. Wissler, S. Quintin, Y. Nagamatsu, S. Sookhareea, F. Landmann, H. Hutter, N. Vitale, and M. Labouesse. 2007. The RhoGAP RGA-2 and LET-502/ROCK achieve a balance of actomyosin-dependent forces in *C. elegans* epidermis to control morphogenesis. *Development.* 134:2469–2479. http://dx.doi.org/10.1242/dev.005074

Duan, L., G. Chen, S. Virmani, G. Ying, S.M. Raja, B.M. Chung, M.A. Rainey, M. Dimri, C.F. Ortega-Cava, X. Zhao, et al. 2010. Distinct roles for Rho versus Rac/Cdc42 GTPases downstream of Vav2 in regulating mammary epithelial acinar architecture. *J. Biol. Chem.* 285:1555–1568. http://dx.doi.org/10.1074/jbc.M109.057976

Engl, W., B. Arasi, L.L. Yap, J.P. Thiery, and V. Viasnoff. 2014. Actin dynamics modulate mechanosensitive immobilization of E-cadherin at adherens junctions. *Nat. Cell Biol.* 16:587–594. http://dx.doi.org/10.1038/ncb2973

Ewald, A.J., A. Brenot, M. Duong, B.S. Chan, and Z. Werb. 2008. Collective epithelial migration and cell rearrangements drive mammary branching morphogenesis. *Dev. Cell.* 14:570–581. http://dx.doi.org/10.1016/j.devcel.2008.03.003

Farooqui, R., and G. Fenteany. 2005. Multiple rows of cells behind an epithelial wound edge extend cryptic lamellipodia to collectively drive cell-sheet movement. *J. Cell Sci.* 118:51–63. http://dx.doi.org/10.1242/jcs.01577

Gally, C., F. Wissler, H. Zahreddine, S. Quintin, F. Landmann, and M. Labouesse. 2009. Myosin II regulation during *C. elegans* embryonic elongation: LET-502/ROCK, MRCK-1 and PAK-1, three kinases with different roles. *Development.* 136:3109–3119. http://dx.doi.org/10.1242/dev.039412

Georgiou, M., and B. Baum. 2010. Polarity proteins and Rho GTPases cooperate to spatially organise epithelial actin-based protrusions. *J. Cell Sci.* 123:1089–1098. http://dx.doi.org/10.1242/jcs.060772

Gibson, W.T., and M.C. Gibson. 2009. Cell topology, geometry, and morphogenesis in proliferating epithelia. *Curr. Top. Dev. Biol.* 89:87–114. http://dx.doi.org/10.1016/S0070-2153(09)89004-2

Gibson, M.C., A.B. Patel, R. Nagpal, and N. Perrimon. 2006. The emergence of geometric order in proliferating metazoan epithelia. *Nature.* 442:1038–1041. http://dx.doi.org/10.1038/nature05014

Guilluy, C., R. Garcia-Mata, and K. Burridge. 2011. Rho protein crosstalk: Another social network? *Trends Cell Biol.* 21:718–726. http://dx.doi.org/10.1016/j.tcb.2011.08.002

Heid, P.J., W.B. Raich, R. Smith, W.A. Mohler, K. Simokat, S.B. Gendreau, J.H. Rothman, and J. Hardin. 2001. The zinc finger protein DIE-1 is required for late events during epithelial cell rearrangement in *C. elegans*. *Dev. Biol.* 236:165–180. http://dx.doi.org/10.1006/dbio.2001.0315

Jilkine, A., A.F. Marée, and L. Edelstein-Keshet. 2007. Mathematical model for spatial segregation of the Rho-family GTPases based on inhibitory crosstalk. *Bull. Math. Biol.* 69:1943–1978. http://dx.doi.org/10.1007/s11538-007-9200-6

Kalaji, R., A.P. Wheeler, J.C. Erasmus, S.Y. Lee, R.G. Endres, L.P. Cramer, and V.M. Braga. 2012. ROCK1 and ROCK2 regulate epithelial polarisation and geometric cell shape. *Biol. Cell.* 104:435–451. http://dx.doi.org/10.1111/boc.201100093

Kamath, R.S., and J. Ahringer. 2003. Genome-wide RNAi screening in *Caenorhabditis elegans*. *Methods.* 30:313–321. http://dx.doi.org/10.1016/S1046-2023(03)00050-1

Keller, R. 2006. Mechanisms of elongation in embryogenesis. *Development.* 133:2291–2302. http://dx.doi.org/10.1242/dev.02406

Kuo, J.C., X. Han, C.T. Hsiao, J.R. Yates III, and C.M. Waterman. 2011. Analysis of the myosin-II-responsive focal adhesion proteome reveals a role for β-Pix in negative regulation of focal adhesion maturation. *Nat. Cell Biol.* 13:383–393. http://dx.doi.org/10.1038/ncb2216

Lecuit, T., and A.S. Yap. 2015. E-cadherin junctions as active mechanical integrators in tissue dynamics. *Nat. Cell Biol.* 17:533–539. http://dx.doi.org/10.1038/ncb3136

Levayer, R., A. Pelissier-Monier, and T. Lecuit. 2011. Spatial regulation of Dia and Myosin-II by RhoGEF2 controls initiation of E-cadherin endocytosis during epithelial morphogenesis. *Nat. Cell Biol.* 13:529–540. http://dx.doi.org/10.1038/ncb2224

Lewis, F.T. 1928. The correlation between cell division and the shapes and sizes of prismatic cells in the epidermis of *Cucumis*. *Anat. Rec.* 38:341–376. http://dx.doi.org/10.1002/ar.1090380305

Liu, F., L. Jia, A.M. Thompson-Baine, J.M. Puglise, M.B. Ter Beest, and M.M. Zegers. 2010. Cadherins and Pak1 control contact inhibition of proliferation by Pak1-betaPIX-GIT complex-dependent regulation of cell-matrix signaling. *Mol. Cell. Biol.* 30:1971–1983. http://dx.doi.org/10.1128/MCB.01247-09

Ma, M., and M. Baumgartner. 2013. Filopodia and membrane blebs drive efficient matrix invasion of macrophages transformed by the intracellular parasite *Theileria annulata*. *PLoS One.* 8:e75577. http://dx.doi.org/10.1371/journal.pone.0075577

Martin, E., S. Harel, B. Nkengfac, K. Hamiche, M. Neault, and S. Jenna. 2014. pix-1 controls early elongation in parallel with mel-11 and let-502 in *Caenorhabditis elegans*. *PLoS One.* 9:e94684. http://dx.doi.org/10.1371/journal.pone.0094684

Maruthamuthu, V., B. Sabass, U.S. Schwarz, and M.L. Gardel. 2011. Cell-ECM traction force modulates endogenous tension at cell-cell contacts. *Proc. Natl. Acad. Sci. USA.* 108:4708–4713. http://dx.doi.org/10.1073/pnas.1011123108

Munjal, A., and T. Lecuit. 2014. Actomyosin networks and tissue morphogenesis. *Development.* 141:1789–1793. http://dx.doi.org/10.1242/dev.091645

Nakamura, F. 2013. FilGAP and its close relatives: A mediator of Rho-Rac antagonism that regulates cell morphology and migration. *Biochem. J.* 453:17–25. http://dx.doi.org/10.1042/BJ20130290

Nayal, A., D.J. Webb, C.M. Brown, E.M. Schaefer, M. Vicente-Manzanares, and A.R. Horwitz. 2006. Paxillin phosphorylation at Ser273 localizes a GIT1-PIX-PAK complex and regulates adhesion and protrusion dynamics. *J. Cell Biol.* 173:587–589. http://dx.doi.org/10.1083/jcb.200509075

Ohta, Y., J.H. Hartwig, and T.P. Stossel. 2006. FilGAP, a Rho- and ROCK-regulated GAP for Rac binds filamin A to control actin remodelling. *Nat. Cell Biol.* 8:803–814. http://dx.doi.org/10.1038/ncb1437

Pásti, G., and M. Labouesse. 2014. Epithelial junctions, cytoskeleton, and polarity. *WormBook.* 1–35. http://dx.doi.org/10.1895/wormbook.1.56.2

Peng, H., Z. Ruan, F. Long, J.H. Simpson, and E.W. Myers. 2010. V3D enables real-time 3D visualization and quantitative analysis of large-scale biological image data sets. *Nat. Biotechnol.* 28:348–353. http://dx.doi.org/10.1038/nbt.1612

Pertz, O. 2010. Spatio-temporal Rho GTPase signaling—where are we now? *J. Cell Sci.* 123:1841–1850. http://dx.doi.org/10.1242/jcs.064345

Piekny, A.J., A. Wissmann, and P.E. Mains. 2000. Embryonic morphogenesis in *Caenorhabditis elegans* integrates the activity of LET-502 Rho-binding kinase, MEL-11 myosin phosphatase, DAF-2 insulin receptor and FEM-2 PP2c phosphatase. *Genetics.* 156:1671–1689.

Piekny, A.J., J.L. Johnson, G.D. Cham, and P.E. Mains. 2003. The *Caenorhabditis elegans* nonmuscle myosin genes nmy-1 and nmy-2 function as redundant components of the let-502/Rho-binding kinase and mel-11/myosin phosphatase pathway during embryonic morphogenesis. *Development.* 130:5695–5704. http://dx.doi.org/10.1242/dev.00807

Pirraglia, C., J. Walters, and M.M. Myat. 2010. Pak1 control of E-cadherin endocytosis regulates salivary gland lumen size and shape. *Development.* 137:4177–4189. http://dx.doi.org/10.1242/dev.048827

Plutoni, C., E. Bazellieres, M. Le Borgne-Rochet, F. Comunale, A. Brugues, M. Séveno, D. Planchon, S. Thuault, N. Morin, S. Bodin, et al. 2016. P-cadherin promotes collective cell migration via a Cdc42-mediated increase in mechanical forces. *J. Cell Biol.* 212:199–217. http://dx.doi.org/10.1083/jcb.201505105

Priess, J.R., and D.I. Hirsh. 1986. *Caenorhabditis elegans* morphogenesis: The role of the cytoskeleton in elongation of the embryo. *Dev. Biol.* 117:156–173. http://dx.doi.org/10.1016/0012-1606(86)90358-1

Rauzi, M., P. Verant, T. Lecuit, and P.F. Lenne. 2008. Nature and anisotropy of cortical forces orienting *Drosophila* tissue morphogenesis. *Nat. Cell Biol.* 10:1401–1410. http://dx.doi.org/10.1038/ncb1798

Sailem, H., V. Bousgouni, S. Cooper, and C. Bakal. 2014. Cross-talk between Rho and Rac GTPases drives deterministic exploration of cellular shape space and morphological heterogeneity. *Open Biol.* 4:130132. http://dx.doi.org/10.1098/rsob.130132

Saito, K., Y. Ozawa, K. Hibino, and Y. Ohta. 2012. FilGAP, a Rho/Rho-associated protein kinase-regulated GTPase-activating protein for Rac, controls

tumor cell migration. *Mol. Biol. Cell.* 23:4739–4750. http://dx.doi.org/10.1091/mbc.E12-04-0310

Semplice, M., A. Veglio, G. Naldi, G. Serini, and A. Gamba. 2012. A bistable model of cell polarity. *PLoS One.* 7:e30977. http://dx.doi.org/10.1371/journal.pone.0030977

Symons, M., and J.E. Segall. 2009. Rac and Rho driving tumor invasion: Who's at the wheel? *Genome Biol.* 10:213. http://dx.doi.org/10.1186/gb-2009-10-3-213

Tsyganov, M.A., W. Kolch, and B.N. Kholodenko. 2012. The topology design principles that determine the spatiotemporal dynamics of G-protein cascades. *Mol. Biosyst.* 8:730–743. http://dx.doi.org/10.1039/c2mb05375f

Vaezi, A., C. Bauer, V. Vasioukhin, and E. Fuchs. 2002. Actin cable dynamics and Rho/Rock orchestrate a polarized cytoskeletal architecture in the early steps of assembling a stratified epithelium. *Dev. Cell.* 3:367–381. http://dx.doi.org/10.1016/S1534-5807(02)00259-9

Vargo-Gogola, T., B.M. Heckman, E.J. Gunther, L.A. Chodosh, and J.M. Rosen. 2006. P190-B Rho GTPase-activating protein overexpression disrupts ductal morphogenesis and induces hyperplastic lesions in the developing mammary gland. *Mol. Endocrinol.* 20:1391–1405. http://dx.doi.org/10.1210/me.2005-0426

Vicente-Manzanares, M., K. Newell-Litwa, A.I. Bachir, L.A. Whitmore, and A.R. Horwitz. 2011. Myosin IIA/IIB restrict adhesive and protrusive signaling to generate front-back polarity in migrating cells. *J. Cell Biol.* 193:381–396. http://dx.doi.org/10.1083/jcb.201012159

Vlachos, S., and N. Harden. 2011. Genetic evidence for antagonism between Pak protein kinase and Rho1 small GTPase signaling in regulation of the actin cytoskeleton during *Drosophila* oogenesis. *Genetics.* 187:501–512. http://dx.doi.org/10.1534/genetics.110.120998

Walck-Shannon, E., D. Reiner, and J. Hardin. 2015. Polarized Rac-dependent protrusions drive epithelial intercalation in the embryonic epidermis of C. elegans. *Development.* 142:3549–3560. http://dx.doi.org/10.1242/dev.127597

Weber, G.F., M.A. Bjerke, and D.W. DeSimone. 2012. A mechanoresponsive cadherin-keratin complex directs polarized protrusive behavior and collective cell migration. *Dev. Cell.* 22:104–115. http://dx.doi.org/10.1016/j.devcel.2011.10.013

Williams, M., W. Yen, X. Lu, and A. Sutherland. 2014. Distinct apical and basolateral mechanisms drive planar cell polarity-dependent convergent extension of the mouse neural plate. *Dev. Cell.* 29:34–46. http://dx.doi.org/10.1016/j.devcel.2014.02.007

Williams-Masson, E.M., A.N. Malik, and J. Hardin. 1997. An actin-mediated two-step mechanism is required for ventral enclosure of the *C. elegans* hypodermis. *Development.* 124:2889–2901.

Williams-Masson, E.M., P.J. Heid, C.A. Lavin, and J. Hardin. 1998. The cellular mechanism of epithelial rearrangement during morphogenesis of the *Caenorhabditis elegans* dorsal hypodermis. *Dev. Biol.* 204:263–276. http://dx.doi.org/10.1006/dbio.1998.9048

Wyckoff, J.B., S.E. Pinner, S. Gschmeissner, J.S. Condeelis, and E. Sahai. 2006. ROCK- and myosin-dependent matrix deformation enables protease-independent tumor-cell invasion in vivo. *Curr. Biol.* 16:1515–1523. http://dx.doi.org/10.1016/j.cub.2006.05.065

Yamazaki, D., S. Kurisu, and T. Takenawa. 2009. Involvement of Rac and Rho signaling in cancer cell motility in 3D substrates. *Oncogene.* 28:1570–1583. http://dx.doi.org/10.1038/onc.2009.2

Yashiro, H., A.J. Loza, J.B. Skeath, and G.D. Longmore. 2014. Rho1 regulates adherens junction remodeling by promoting recycling endosome formation through activation of myosin II. *Mol. Biol. Cell.* 25:2956–2969. http://dx.doi.org/10.1091/mbc.E14-04-0894

Yin, Z., A. Sadok, H. Sailem, A. McCarthy, X. Xia, F. Li, M.A. Garcia, L. Evans, A.R. Barr, N. Perrimon, et al. 2013. A screen for morphological complexity identifies regulators of switch-like transitions between discrete cell shapes. *Nat. Cell Biol.* 15:860–871. http://dx.doi.org/10.1038/ncb2764

Yu, W., L.E. O'Brien, F. Wang, H. Bourne, K.E. Mostov, and M.M. Zegers. 2003. Hepatocyte growth factor switches orientation of polarity and mode of movement during morphogenesis of multicellular epithelial structures. *Mol. Biol. Cell.* 14:748–763. http://dx.doi.org/10.1091/mbc.E02-06-0350

Zallen, J.A. 2007. Planar polarity and tissue morphogenesis. *Cell.* 129:1051–1063. http://dx.doi.org/10.1016/j.cell.2007.05.050

Zhang, H., F. Landmann, H. Zahreddine, D. Rodriguez, M. Koch, and M. Labouesse. 2011. A tension-induced mechanotransduction pathway promotes epithelial morphogenesis. *Nature.* 471:99–103. http://dx.doi.org/10.1038/nature09765